UNIVERSITY OF CALIFORNIA

Santa Barbara

Landslides: Geomorphology and Sea Cliff Hazard Potential, Santa Barbara – Isla Vista, California

A Thesis submitted in partial satisfaction of the

requirements for the degree Master of Science

in Earth Science

by

Julia F Klath

Committee in Charge:

Professor Edward A. Keller, Chair

Professor Alexander Simms

Professor Jordan Clark

September 2018

The thesis of Julia F Klath is approved.

Alexander Simms

Jordan Clark

Edward A. Keller, Committee Chair

July 2018

Landslides: Geomorphology and Sea Cliff Hazard Potential, Santa Barbara – Isla Vista, California

ACKNOWLEDGMENTS

Thank you to Ed Keller, and my graduate committee, for your patience and guidance through this process.

In honor of Patricia Klath, Susan Klath, Rhonda Hoose Eastham, Livingston Eastham, Shelia Davis, and Benjamin Ramos. Impactful individuals, gone before their time; collectively they taught me the value of being worthy, kind, driven, and most of all to see the value of being myself.

ABSTRACT

Landslides: Geomorphology and Sea Cliff Hazard Potential, Santa Barbara – Isla Vista, California

by

Julia Klath

Coastal areas are often characterized by high population densities and variable geologic formations. Over 80% of the world's coastal regions are dominated by steeply sloping surfaces (sea cliffs) that are subjected to various erosional and geological processes. Due to the ever changing nature of these areas, a deeper understanding of how these surfaces have changed in the past may enable populations to anticipate future behavior and discover more effective ways to mitigate future coastal hazards. In this study, mapping and analysis of local bedrock morphology and petrology focuses on further understanding the relationship between bedrock lithology and landslide frequency and volume. Using field mapping techniques in conjunction with digital maps and non-parametric comparative statistical methods, a series of landslide characteristics, including landslide volumes and areas, compressive rock strength surrounding landslides, average cliff heights, and bedding dips around landslides, have be collected and analyzed. Four geologically distinct areas exist along the coastal reach between Santa Barbara and Isla Vista, dominated by the Sisquoc shale and subunits of the Monterey Shale. Each unit displays varying lithology, and as a result, each area experiences weathering and failure in different ways.

The underlying lithology and structure of the region influence the nature and extent of landslide activity >100m^3. Generally it has been found that in sections with beds dipping

south, towards the ocean, at >30º there are more landslides per unit area. Based upon sea cliff profile analysis it has also been found that sections with greatest cliff height, >35m, also have distinctive profiles where weathering of rocks above is prevalent, with cliff bases maintaining some bedding structure. The orientation of bedding as well as the dominance of either Si or Ca rich interbeds has an impact on landslide activity. Generally, Ca rich interbeds are more susceptible to weathering than Si rich beds. Lastly it has been noted that when measuring compressive rock strength with a Schmidt hammer, return values may be more indicative of the degree of weathering of the bedrock around a landslide rather than a measure of actual rock compressive strength. Significant variations in return values occur between the cliff base and as little as 0.5m higher up the cliff face. Average strength of cliff bases is recorded for each section and show the lowest values for quaternary units and areas where the bedrock is highly weathered, with higher values occurring where wave action has removed talus materials from the area and has direct access to the cliff bases.

TABLE OF CONTENTS

ACKNOWLEDGMENTS iv
ABSTRACT vi
LIST OF FIGURES viii

LIST OF TABLES viii

INTRODUCTION 1

BACKGROUND 4
Geologic Setting 4
Previous Work 5
Sea Cliff Characteristics 6
Sea Cliff Profiles 8
Rock Strength 11
Field Mapping 11
Study Area 11
Stratigraphic column 15

METHODS 16
Rock Descriptions 16
Detailed Descriptions 16
Aerial Photo Annotation Analysis 21
Field Inventory: Sea Cliff Characteristics 22
Digital Topographic Analysis 22
Landslide Volume Calculations 23
Schmidt Hammer 24
Analysis of Sea Cliff Variables 25
Statistical Methods 25
Kolmogorov-Smirnov Test for Normality 26
Kruskal Wallis H Test 26
Kolmogorov-Smirnov Test 27

RESULTS 28
All Field Mapping Data 29
Landslide Inventory 30
Schmidt Hammer Data Results 36
Cliff Top Sinuosity 38
Sea Cliff Profile Analysis Results 40
Landslide Statistic Results 44
Landslide Characteristics Distributions 44
Kruskal Wallis and Kolmogorov-Smirnov Statistics 52

DISCUSSION 55
Landslide Inventory Synthesis 55

Physical Variables Driving Sea Cliff Failure: a comparison 55
Physical Sea Cliff Variables and Variations; geomorphology and petrology 57
Sisquoc Shale: Section 5 Discussion 58
Future Work 59

CONCLUSIONS 61

REFERENCES 62

APPENDIX 64
Appendix A: Detailed Geologic Maps of Field Area by Section 64

LIST OF FIGURES

Figure Number Page Number

1. Map of the Santa Barbara Region from Santa Barbara point to Coal Oil point..... 1
2. The Santa Barbara Fold Belt, An Overview 4
3. Idealized Diagram of an Archetypal Sea Cliff Along the Santa Barbara Coastline . 6
4. Photographs: Sea Cliff Daylighting Beds 7
5. Idealized Diagram of Sea Cliff Profiles Linked to Natural Processes 9
6. Idealized Diagram of Shore Platform Types Compared to a Plunging Cliff Source 10
7. Santa Barbara Digital Elevation Model Overview Map 13
8. Generalized Composite Stratigraphic Column, Santa Barbara CA..... 15
9. Photo: Sisquoc Formation 18
10. Photo: Monterey Formation, Upper 19
11. Photo: Monterey Formation, Middle..... 20
12. Photo: Monterey Formation, Lower..... 21
13. ArcGIS DEM Landslide Volume Calculation 24
14. Landslide Volume With Distance Along Field Area 34
15. Landslide Correlation Matrix: Analysis of Non-Numerical Data..... 35
16. Photo: Schmidt Hammer Data Collection Example Image..... 36
17. Schmidt Hammer Rebound Values Along Field Area 37
18. Sinuosity Measurement Map Example 39
19. Sea Cliff Profiles for Section 1 41
20. Sea Cliff Profiles for Section 2 41
21. Sea Cliff Profiles for Section 3 42
22. Sea Cliff Profiles for Section 4 42
23. Sea Cliff Profiles for Section 5 43
24. Distributions of Landslide Variables for All Sections 45
25. Distributions of Landslide Volumes with Each Section Plotted Individually 46
26. Distributions of Landslide Areas with Each Section Plotted Individually..... 47
27. Distributions of Landslide Schmidt Hammer Values with Each Section Plotted Individually 48
28. Distributions of Landslide Bedding Dip Values with Each Section Plotted Individually 49
29. Distributions of Landslide Cliff Height Values with Each Section Plotted Individually 50
30. Photo: Sisquoc Shale, Section 5, Hazards Example..... 59

LIST OF TABLES

Table Number Page Number

1. Landslide Data for each mapped location >100m^3 29
2. Landslide Inventory Results..... 31
3. Landslide and Secondary Characteristics by Percent..... 32
4. Cliff Top Sinuosity Results..... 38
5. Kolmogorov-Smirnov Distribution Results 45
6. Kolmogorov-Smirnov Individual Section Distribution Results..... 51

7. Kruskal Wallis Test Results 52
8. Kolmogorov-Smirnov Two-Sample Test Results 54

INTRODUCTION

Coastal areas are often characterized by high population densities in an ever changing, energetic environment. Shaped largely by tectonics, up to 80% of the world's coastlines are dominated by steeply sloping sea cliffs (Emory and Kuhn, 1982), the morphology of which reflects their tectonic setting, rock type, wave erosion, and surface erosion, as well as human activities such as changing vegetation, urban runoff, and construction of coastal defenses. Santa Barbara and Goleta, (the Santa Barbara area) located in coastal southern California, have approximately 26 km of scenic coastline. 17km of sea cliffs and beaches extend from Santa Barbara Point to the hamlet of Isla Vista and Coal Oil Point (Figure 1).

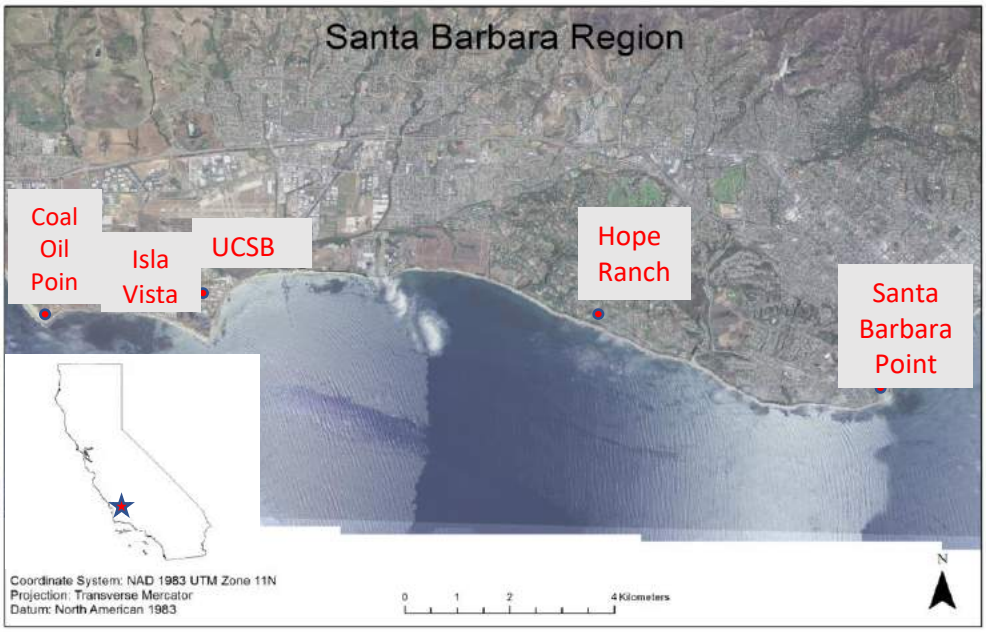

Figure 1. Map of the Santa Barbara region from Santa Barbara point to Coal Oil point. Overview of the entire field area. The base map is a google earth overlay (2015 satellite imagery) available through the ESRI ArcGIS archives.

Within the tectonically active setting of the Santa Barbara fold belt, sea cliffs often manifest as steeply sloped surfaces acted upon by sub aerial and marine processes as well as by human activities. The result is an ever-changing, dynamic coastal system. Sea cliff retreat and landslide events are a continuous challenge for the region, as well as for the University of California – Santa Barbara campus. A deeper understanding of the local geology and the physical processes generating slope failure and thus landward cliff retreat is vital, not only for public safety, but for future development and planning (Hampton and Griggs, 2004). To further understand the mechanics of local slope failure and the magnitude and frequency of failure, it is necessary to take a closer look at local bedrock lithology. Two geologic formations dominate the sea cliffs of the Santa Barbara area: Monterey shale (upper, middle, and lower) and Sisquoc shale (Minor et al., 2009). These units were formed between 5-24 Ma during the Miocene and lower Pliocene epochs. Lithologic variability is low within all rock units and the geology varies from variably weathered cemented shale with or without diatoms and other fossils to mineral veins comprised of silicate rich or calcium rich materials to variably weathered compaction shale. Variations in landslide characteristics are linked closely to the geology of a specific site that affects how easily rock units are weathered and eroded by wave action and other processes. Variations include not only the mineralogy of rock units, but also cliff height, the slope of the cliff surrounding the failure area, the dip of bedding, and the compressive strength of bedrock at a given landslide, as well as the

measured volume and area of a failure. Other features and processes that may contribute to weakening local bedrock (Griggs et al., 2005; Griggs and Russell, 2012) are also categorized and include human based and naturally occurring groundwater seepage (Norris and Back, 1990), drainage installed within the sea cliff accommodating cliff top structures, and beach access structures built into the cliffs (e.g. – stairs, ramps, etc.).

While there exists pronounced differences between the compacted Sisquoc shale and the cemented Monterey shale units, further classifying these rock units is necessary to evaluate hazard potential along the coastline. Quantifying the way these units fail and the differences between how they fail is vital to evaluating hazard potential along these sea cliffs. Data collection and models developed here, coupled with evaluation of past studies, notably Young et al., 2011, and a detailed evaluation of past landslide behaviors, ideally may be used to further develop our understanding of landslide failure along sea cliff dominated coastlines, in Santa Barbara, and around the world.

The purpose of this study is to assess landslide hazard potential along the sea cliffs through the investigation and cataloging of existing landslide events and how these events relate to physical variables (rock type, basic mineralogy,and degree of weathering) and characteristics within the surrounding bedrock, to gain a deeper understanding of landslide hazards along the Santa Barbara coastline. Specifically, how rock type and accompanying physical attributes contribute to landslide volume and frequency.

BACKGROUND

Geologic Setting

The geomorphology of the Santa Barbara coastline is in large part due to the location of anticlines and synclines (Keller and Gurrola, 2000; Gurrola et al., 2014). The area lies within the highly active geologic setting of the western United States, amidst the greater tectonic compressional setting caused by the left bend in the San Andreas fault, along the southern edge of the Western Transverse ranges within the active Santa Barbara fold belt (SBFB) and is shaped by a series of folds and faults (Figure 2). Generally, low lying areas are associated with faulted synclines (e.g.- the city of Santa Barbara) with hills and higher topography associated with anticlines. These anti clines are thought to be actively uplifting and have thus, along with erosional processes, exposed and generated a series of marine terraces (Keller and Gurrola 2000; Keller et al., 2007).

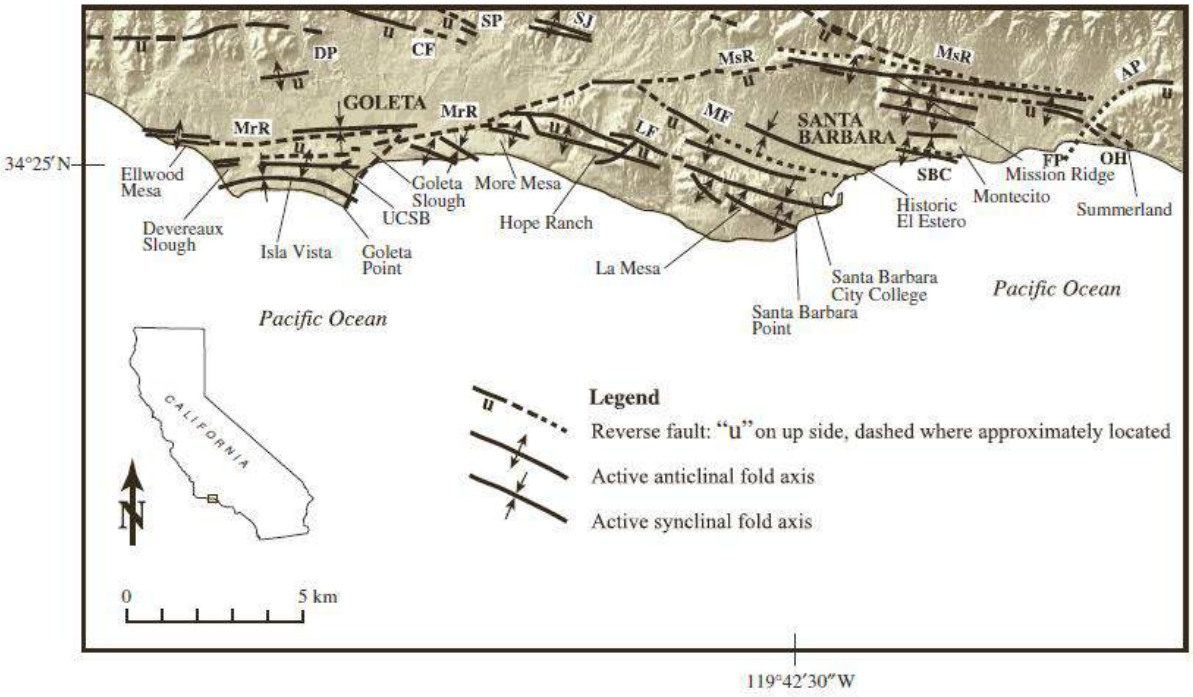

Figure 2. The Santa Barbara fold belt. Source: Gurrola et al, 2014. Anticlinal and synclinal

features responsible for exposed marine terraces are shown and reveal the resulting geomorphology of the Santa Barbara area coastline.

These anticlines fold and uplift marine terraces forming the sea cliffs within the field area. The terraces are generally expressed as uplifted wave cut platforms on Monterey and Sisquoc Shale of variable thickness from 5-50m. Ages of the units vary from 4-16 Ma; they are covered with a layer of beach and/or terrestrial sediment that varies in thickness, from 1±3m and age (40-80 Ka). Units also express various uplift rates (0.5-2m/ky). Estimates of uplift rates calculated by Gurrola et al., 2014 show the highest rates near More Mesa and westward of about 2m/ky.

Previous Work

Past erosion/retreat rates for the California coastline have been studied thoroughly (e.g.- Norris, 1990; Griggs et al., 2005; Hapke et al., 2009; Parrish, 2008) and analyses and projections show that the Santa Barbara region has been susceptible to moderate rates of sea cliff erosion in the past and is currently undergoing active, sometimes rapid, erosion. Cliff retreat is variable along the field area with higher rates existing along the More Mesa preserve area at an average of 15-23 cm/yr and throughout campus point into Isla Vista at 7-23 cm/yr (Sylvester, 2016, Griggs et al., 2005). The episodic nature of cliff failure (Griggs et al., 2005) and variability of resistant and erodible bedding explains the large range in retreat values. It should also be noted that wave action works to remove stabilizing landslide toe materials where waves have direct access to cliff bases, most commonly where narrow beaches are present, resulting in higher rates along More Mesa and Isla Vista.

Sea Cliff Characteristics

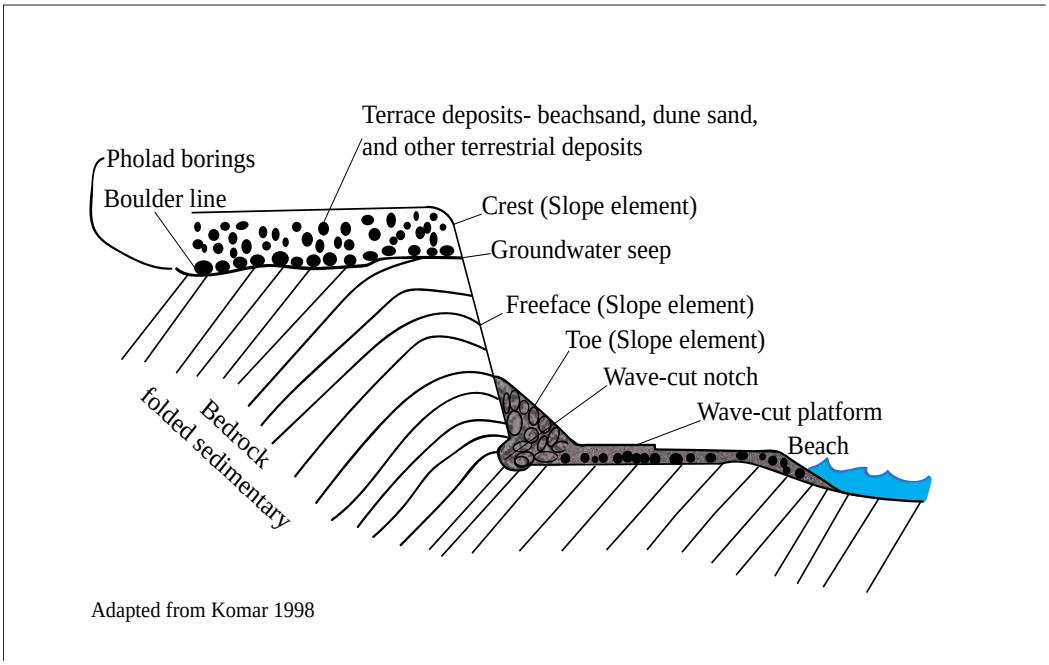

Figure 3. Idealized diagram of an archetypal sea cliff along the Santa Barbara coastline. Source: modified from Komar, 1998.

Along the Santa Barbara coastline, overlying terrestrial deposits may contribute to slope failure through increased overburden pressure on underlying bedrock and groundwater seeps (Figure 3). Hydrologic processes facilitate landslides (Komar, 1998). The permeability and hydraulic conductivity of terrestrial materials is greater than that of marine based shales (USDA, 2012). Therefore, water is able to permeate through overlying sediments and upon reaching the low permeability boundary, infiltration slows and water is only able to permeate into existing joints and cracks within the bedrock. This creates an increase of pore fluid pressure between overlying sediments and bedrock as well as between individual bedrock bedding planes (Van Asch et al., 1999; Blake et al., 2002). Failure may occur with overlying sediments slipping along the low conductivity boundary or by individual beds failing due to

groundwater infiltration. The folded nature of bedding in the field area due to active tectonics is also shown; this can result in

a dip slope condition that may contribute to failure (Griggs and Russell, 2012). Bedding dips in the direction of slope, towards the beach; unsupported bedding planes are exposed and susceptible to sliding, especially where active groundwater seeps are present (Figure 4). Lastly, the diagram illustrates the paleo marine cut platform upon which terrestrial and beach sediments collect; the actively forming and uplifting wave cut platform at sea level, and stabilizing landslide toe materials collecting at sea cliff bases until their subsequent removal by wave action.

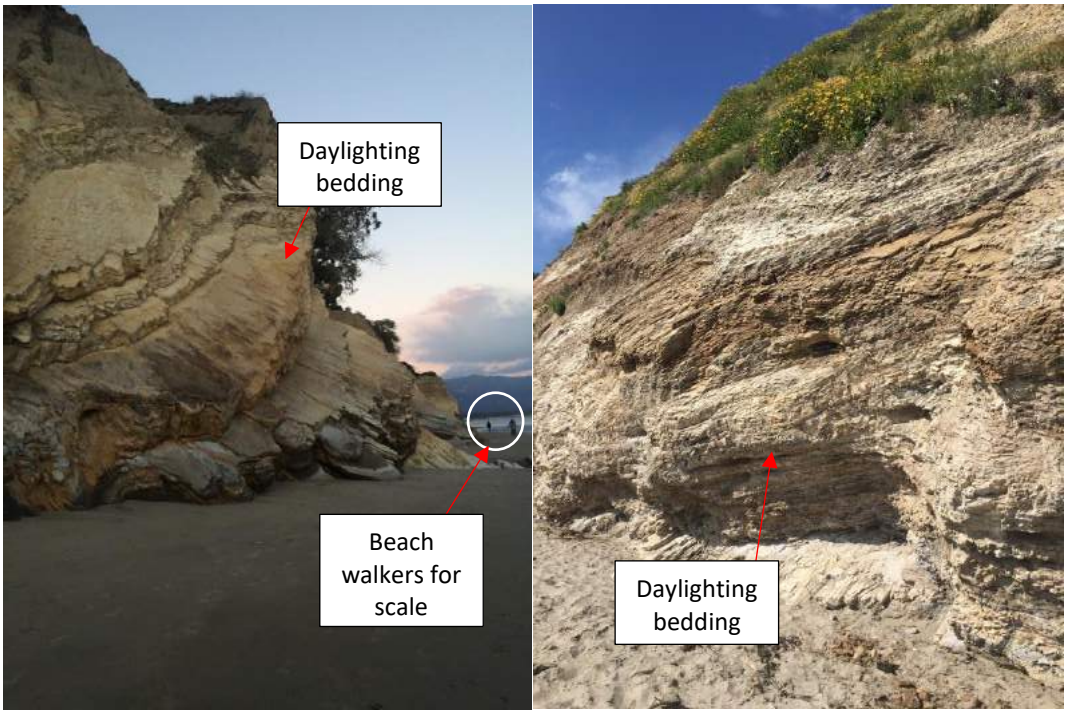

Figure 4. Daylighting bedding (dip slope condition) examples in Tml (left image) and Tmu (right image). Photos: left Shoreline park east end stairs, right 1 km west of Arroyo Burro beach; Photos: Klath, 2015.

Sea Cliff Profiles

The morphology and resultant profile of sea cliffs can yield insight into the dominant erosional forces at work on the cliffs. Emory and Kuhn, 1982 explored the overall shape, or profile of sea cliffs as being indicative of either marine, sub aerial, or both processes acting on them. Throughout the field area, cliffs that have uplifted above the influence of marine weathering and are acted almost exclusively on by sub aerial processes have a rounded, s-type shape while cliffs undergoing marine based weathering have a steeper profile (Figure 5). Examples of sub aerial processes include groundwater runoff and infiltration, bioturbation, vegetation; Human activities can also lead to erosion and include irrigation, construction, and planting. Examples of marine processes include salt spray, wave splash, storm surges (seasonally dependent), and tidal variations. Areas where a wider beach is present will act as a protective barrier for sea cliffs from direct wave attack and allow protective talus to build at sea cliff bases.

Landslide distributions along the coastline are controlled by both physical and structural features within the cliffs and external forces acting upon them. Sunamura, 2015 describes rocky coastlines being classified as either shore platforms or plunging cliffs (Figure 6). Shore platform are further classified as Type-A and Type-B platforms. The soft rocky coastline along the field area is best classified as a Type-A platform. These platforms typically form under the influence of marine weathering; waves undercut easily eroded sea cliff bases, instability results in landslide failure and a temporary stabilization from talus debris forms a protective toe. This toe is ultimately washed away by continual wave action and cliff recession continues. Areas along the field area can be categorized in this way e.g. – steep cliffs with an adjacent beach <10m, however other areas, previously acted upon by

marine processes, have uplifted beyond the influence of waves, are accompanied by a wider beach >10m, and are dominated by sub aerial weathering. Landslides along these areas may be attributed to degree of weathering, formation of joints and cracks within bedding, and orientation of bedding. Overall, erosion, whether by marine or sub aerial processes, can be linked closely to rock type and the competency of the rock unit (Emory and Kuhn, 1982; Griggs et al 2005; Bird, 2016).

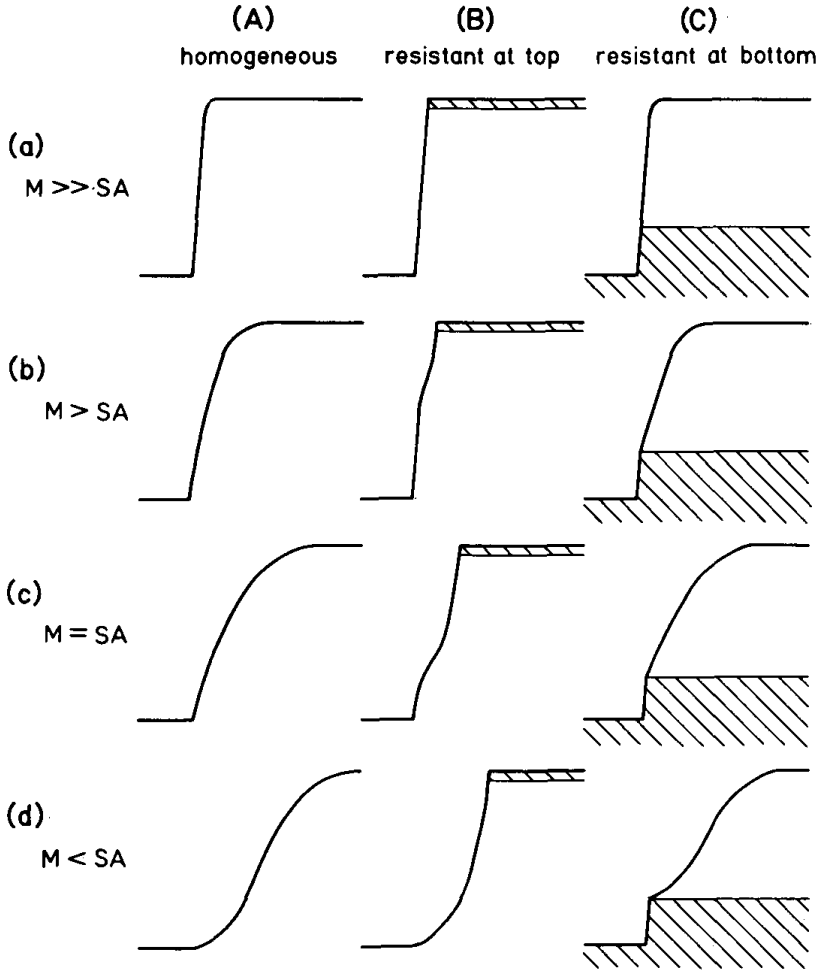

Figure 5. Idealized diagram of sea cliff profiles linked to processes. Source: Emory and Kuhn, 1982. Sea cliff profiles are linked to the processes acting upon them; marine (M) and terrestrial (SA) processes compete in contributing to cliff erosion and morphology, and mass wasting.

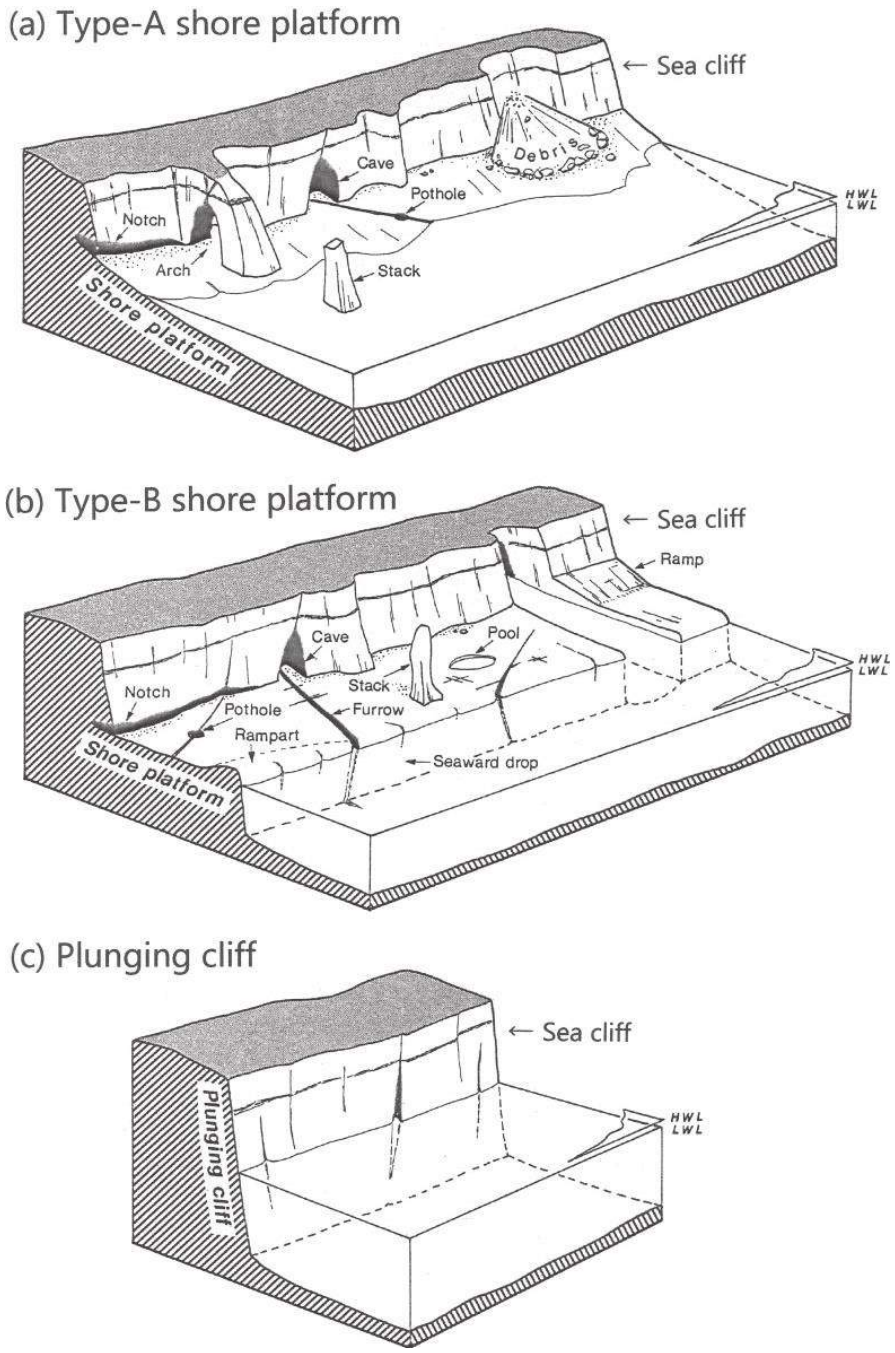

Figure 6. Idealized diagram of shore platform types compared to a plunging cliff source. Source: Sunamura, 2015. The study categorizes soft rock sea cliffs into platforms or plunging cliffs. The field area is best identified as a Type A platform and is characterized by seas cliff base notches, caves, and landslides. HWL = high water line, LWL = low water line.

Rock Strength

Rock strength was measured throughout the study area using a Schmidt Hammer. Previous studies (Duvall et al., 2004; Keller et al., 2015) have employed the use of this tool to assess the compressive strength of materials within the SBFB. Mean rebound values were reported for the Sisquoc and Monterey shales by Duvall et al., 2004; overall, these units are classified as "less resistant" with a value of 23.4 ± 4.1. They also report a mean rebound value of 30.8 ± 1.6 for the Monterey. This value will vary significantly by location due to the Monterey's variable lithology. Rock strength is also controlled by joints and fractures within the bedrock; where cracks and joints are present, a lower rebound value is obtained, as observed in the field.

Field Mapping

The geologic map of the Santa Barbara area by Minor et al., 2009 was referenced extensively while field mapping. Previously mapped landslide locations on the geologic map were noted during sea cliff surveys and proved useful in further classifying and mapping landslides, both older and currently active. Strike and dip of bedding planes were referenced and cross checked against observations made during field mapping.

Study Area

The field area (Figure 7) is located along the coast of Santa Barbara and Goleta in southern California. The coastline studied covers approximately 17km, beginning at the western edge at Coal Oil Point, running east through Isla Vista, the University of California at Santa Barbara (UCSB) campus, and terminating at the eastern boundary by Santa Barbara

Point (Figure 7). The field area is divided into five sections, delineated by the dominant rock type comprising the sea cliffs within each area. Section 1 is 2km in length, dominated by lower Monterey formation shale (Tml), extending from Santa Barbara point to the Santa Barbara lighthouse. Section 2 is 4.8km in length, dominated by middle Monterey formation shale (Tmm), extending from the lighthouse to the contact with the upper Monterey formation shale (Tmu) near Hope Ranch, Ca. Section 3 is 1.4km in length, dominated by Tmu, extending between Hope Ranch and More Mesa. Section 4 is 2.8km in length and is dominated by Sisquoc formation shale (Tsq) overlain by younger, Santa Barbara formation Quaternary age sediments, extending along the More Mesa wildlife preserve into Goleta, terminating at the western edge of Goleta beach with a contact between Tsq and Tmu. Section 5 is 5.9km in length, dominated by Tsq and extends along the UCSB campus and Isla Vista, terminating at Coal Oil Point.

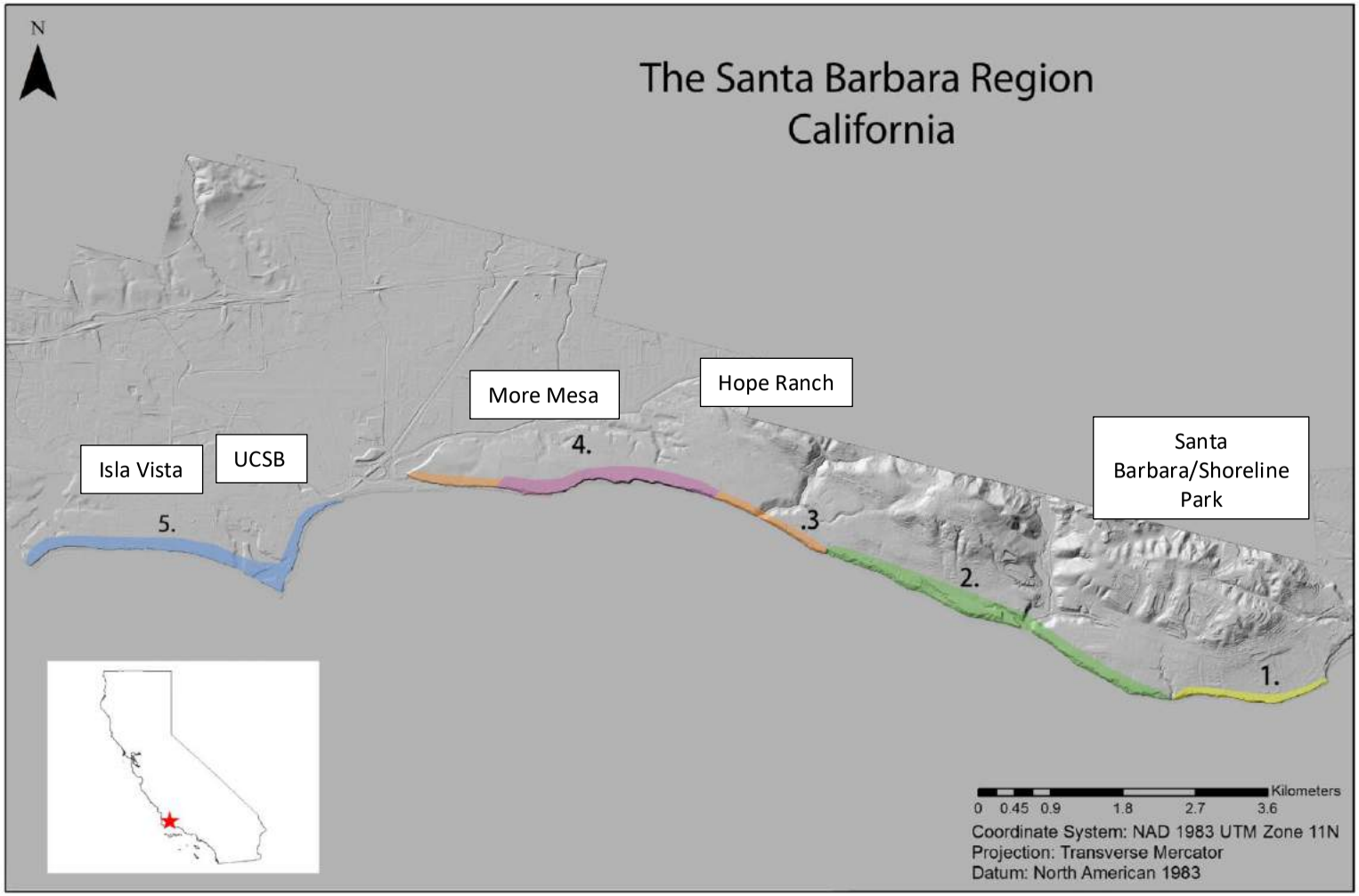
N
The Santa Barbara Region
California
More Mesa
Hope Ranch
Isla Vista
UCSB
Santa Barbara/Shoreline Park
4.
5.
.3
2.
1.
Kilometers
0 0.45 0.9 1.8 2.7 3.6
Coordinate System: NAD 1983 UTM Zone 11N
Projection: Transverse Mercator
Datum: North American 1983

Figure 7. Digital elevation map of the Santa Barbara region in California. The highlighted areas represent the field area extent and the different sections, delineated by rock type. Section 1, yellow, dominated by lower Monterey (Tml). Section 2, green, dominated by middle Monterey (Tmm). Section 3, orange, dominated by upper Monterey (Tmu). Section 4, purple, dominated by Sisquoc and Quaternary units (Tsq/Qs). Section 5, blue, dominated by Sisquoc formation (Tsq). Map source: CA Coastal Conservancy 1-m LiDAR DEM, 2011; Carignan et al., 2009

Studies of the Monterey conducted in past decades focused on oil play potential in the area. As a result, MacKinnon, 1989; Blueford, 1989, and others conducted detailed surveys of local lithology throughout the Californian southern central coast into the Ventura fold belt. They divided, where visible, the Monterey into 5 distinct sections instead of simply lower, middle, and upper (Figure 8). For the purposes of this study, the transitionary phases between the lower and upper Monterey have been included with the middle Monterey after Minor et al., 2009.

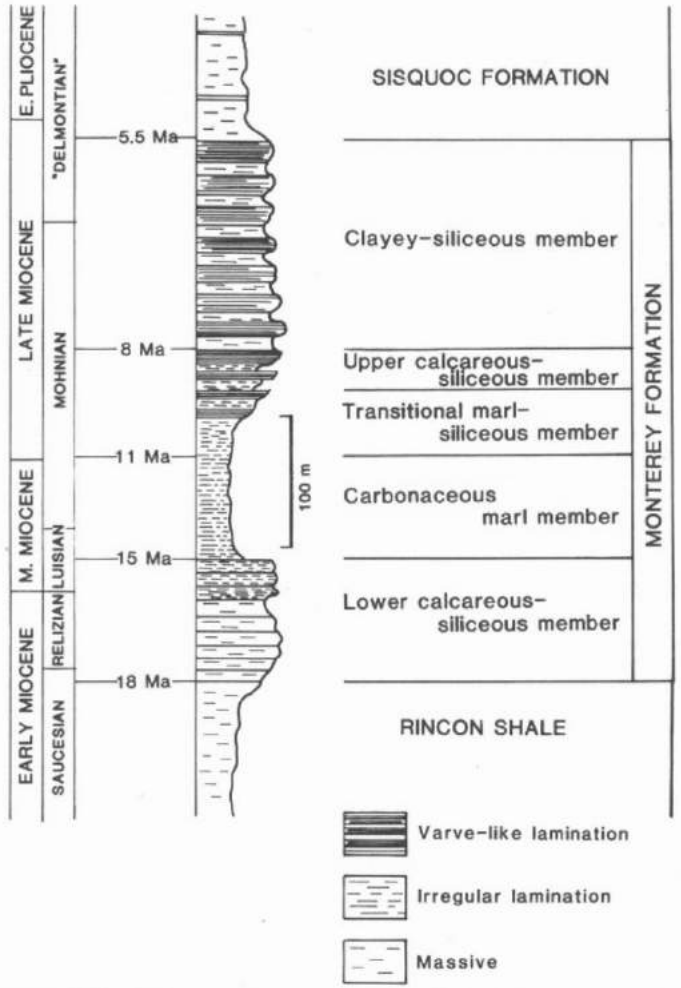

INFERRED ORIGINAL SEDIMENTS (AND GENERALIZED LITHOLOGY), SANTA BARBARA COASTAL AREA

Diatomaceous clay ooze. (Siliceous mudstone/shale, minor porcelanite, cherty porcelanite, dolostone; mainly massive.)	Sisquoc Fm.
Laminated diatomaceous ooze and massive diatomaceous clay ooze. (Porcelanite, siliceous shale/mudstone, minor dolostone and cherty porcelanite)	Monterey Formation
Laminated coccolith-foraminiferal diatomaceous ooze. (Calcareous porcelanite, chert, siliceous shale, locally dolomitic; minor dolostone; glassy chert locally abundant; apatite in lower part.)	
Laminated coccolith-foramiferal ooze. (Marl and chalk, locally dolomitic; minor dolostone, limestone, glassy chert; apatite abundant in some beds.)	
Massive coccolith-foraminiferal diatomaceous ooze. (Calcareous siliceous shale/mudstone, porcelanite, chert, locally dolomitic; apatite in upper part; minor sandstone locally; basal bentonite or volcanoclastic sandstone locally.)	
Clay ooze. (Mudstone and shale, minor dolomite)	Rincon Sh.

Figure 8. Generalized composite stratigraphic column of the Monterey and Sisquoc formations. Note the sub units of the Monterey (Tml is the lower calcareous-siliceous member, Tmm the carbonaceous-transitional-calcareous member, and Tmu clayey-siliceous member), weathering patterns, and dominant petrologic components of each unit. Source: Blueford et al., 1989.

METHODS

Rock Descriptions

The majority of exposed sea cliffs are dominated by Monterey Shale, divided into three distinct subunits (Tml, Tmm, Tmu) that display variation in lithology and bedding orientation. The remainder of the field area covering UCSB and into Isla Vista to Coal Oil Point is primarily Sisquoc Shale (Tsq) displaying significantly less variability than the Monterey. Quaternary units of the Santa Barbara formation overly bedrock throughout the field area but are most notable through the More Mesa area east of Goleta Beach. Rock descriptions are compiled using current field observations and supplemented with previous field mapping by Minor et al., 2009. It should be noted that rock descriptions from Minor tend to lump units and focuses on the larger scale geology of the Santa Barbara region. Rock descriptions below focus in on smaller scale geology within the field area and Minor's unit descriptions are used primarily to confirm field observations.

Detailed descriptions:

Qas, Asphalt (tar) deposits, Holocene. Hardened, weathered tar from surrounding tar seeps. In some places tar covers beach sand or is in turn covered by beach sand, depending on the season. Most notable occurrence is east of Goleta pier between Goleta beach and More

Mesa. Cracks in the primary bedrock are filled with older, partially crystallized Qas deposits throughout the field area, most notably between Shoreline Park and the east end of Arroyo Burro park.

Qmt, Marine terrace deposits, Upper Pleistocene. Qmt unconformably overlies the primary bedrock throughout the field area. Depending upon location, color may vary from buff tan to brown to light gray. Thickness also varies with location from ~3-5 meters. A basal fossil rich layer, generally no more than 1m thick, grades into a massive dune sand/sandstone and/or dark soil layer. Generally unconsolidated and loose/crumbly.

Qcg, Conglomerate unit, Middle-Lower Pleistocene. Rounded, poorly sorted and cemented clasts (fine sand to boulder sized) within a sand matrix. Possible imbrication evident in some places. Bioturbation evident in some places. Approximate thickness of unit ~20m

Qss, Sandstone, Pleistocene. Gray to tan/pink tan, weathered surfaces appear lighter tan. Pink tinge suggests feldspathic sandstone component. Includes minor (<5%) conglomerate bedding and sparse fossils scattered throughout. Minor occurrences of bioturbation along section. Moderate to massive bedding. Total thickness of unit ~ 30m.

QTst, Siltstone, Pleistocene/Pliocene. Contact with Qss vegetated as is 75% of the visible outcrop. Dark gray to brown, lighter brown on weathered surfaces. Poorly bedded, well sorted, where visible. Sparse shell and dolomite fragments visible (<2%). Thickness of unit unclear.

Tsq, Sisquoc formation, Pliocene/Miocene (Figure 9). Marine based, brittle, compacted mudstone/shale, poorly bedded with minor conglomerate bedding throughout. Unit appears darker tan/gray at the base and becomes lighter tan moving upwards, weathered surfaces appear lighter tan. Presence of fossils at the contact between Qmt approximately <1m thick.

Average unit thickness in the field area ~10m except near More Mesa where thickness averages 20-25m. Oxidation staining due to the presence of tar seeps is very low <1%. Oxidation increases within the Monterey formations which has a large, well established oil play.

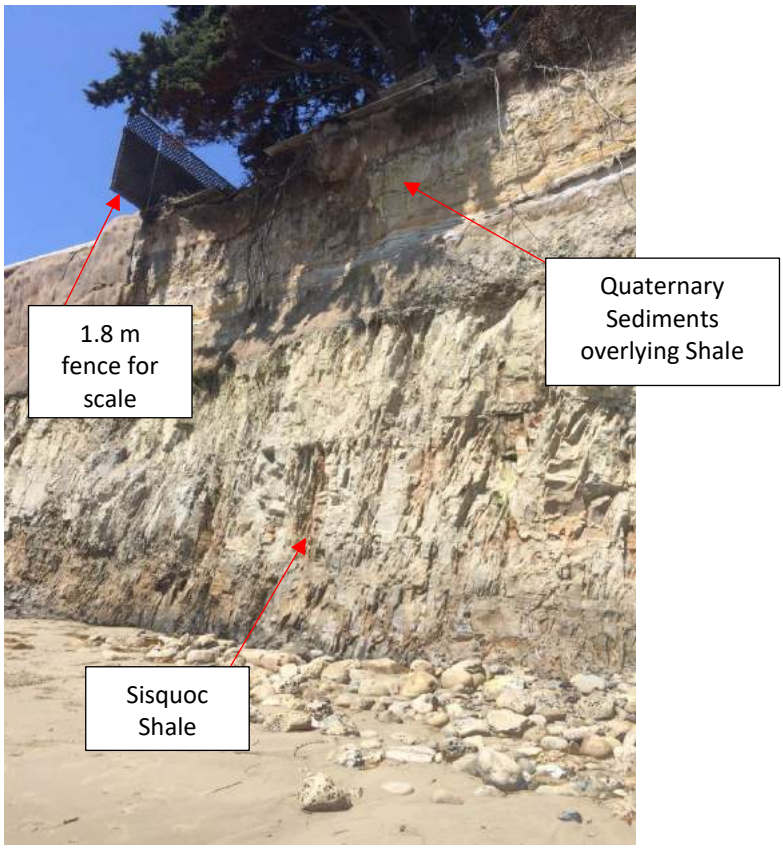

Figure 9. Image of Sisquoc shale with overlying quaternary paleo dune deposits. 1.8m fence for scale. Isla Vista/UCSB boundary. Photo: Klath 2015.

Monterey formation, Miocene. Marine based, cemented, mudstone/shale, well bedded with both siliceous and calcareous beds present; minor dolomite and bentonite veins and lenses. The unit is high in organic content and as such has a high potential for hydrocarbons. The Monterey is exposed most notably within local sea cliffs and dominates 70% of the field

area. Three subunits, distinct in age and lithology, are present within the Monterey. These units have undergone significant deformation and in many cases a dip slope condition exists creatin opportunities for failure along bedding planes (Griggs and Russel, 2005) compounded by groundwater infiltration which may increase local fluid pore pressure resulting in further compromising the ability of these units to resist failure.

Tmu, upper Miocene. Siliceous unit (Figure 10). Brown to gray on fresh surfaces weathering to lighter brown/tan, oxidation staining from tar seeps present. Weak reaction to dilute HCl over several hundred meters, testing every ~100m on sections approximately 1-2 m vertically. Very well bedded (~1-30 mm thick). Abundant fossils and fossil fragments with minor (<5%) dolomite. Vertical thickness of unit within field area 10-15m.

Figure 10. Image of the upper Monterey. Note the steep bedding dip and the laminate like nature of failure. Photo: Klath 2015, Goleta beach (east end).

Tmm, middle Miocene. Mixture of siliceous and calcareous bedding (Figure 11). Very well bedded (~10-30cm with occasional bed >50cm thick). Oxidation staining from tar seeps present as well as abundant porcellanite beds. Evidence of burnt shale noted in several locations. Calcareous beds delineated from siliceous beds based on reaction to dilute HCl. Light to dark variations of banding within bedding depending on composition (Si or Ca rich). Strata generally appear thinly laminated (<0.1m) throughout the unit. Weathered surfaces tend to be lighter tan to white. Mineralized paleo tar seeps are abundant ~ 300m east of Arroyo Burro beach and infill cracks present in mudstone/shale. Presence of fossils, dolomite, tuff, and opal/quartz noted by Minor et al., 2009. Thickness of unit within field area 10-30m. Unit fails as large, voluminous landslides and appears generally more weathered than other Monterey units.

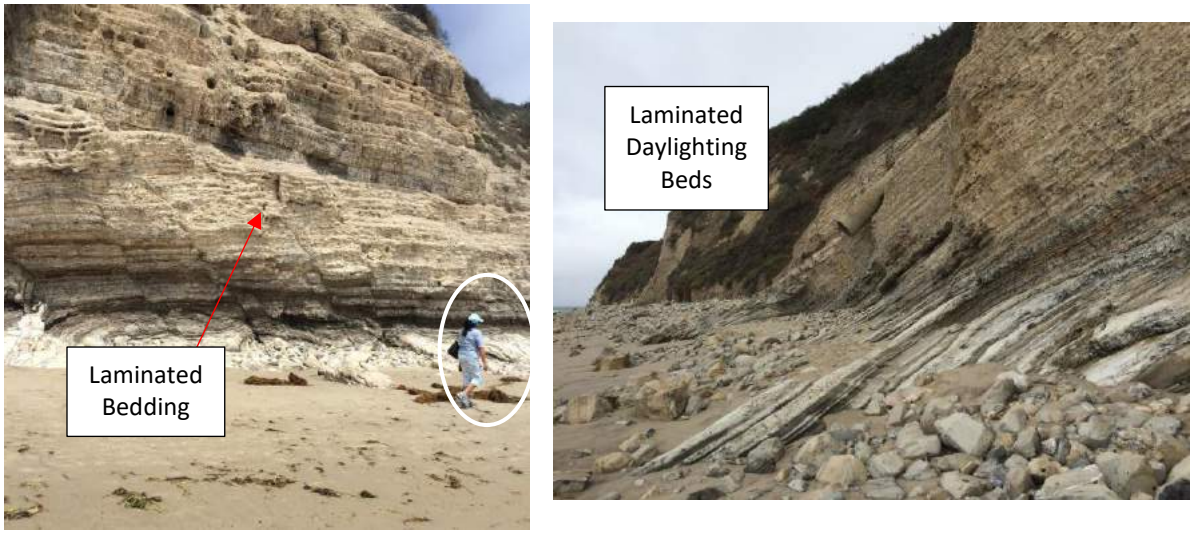

Figure 11. Image of a section of middle Monterey. Rock unit displays great compositional and structural variety; highly weathered in most locations. Left: 0.8 km west of Arroyo Burro

beach, woman (162 cm, circled) for scale. Right: 1.6 km east of Arroyo Burro beach, note drainage pipe inserted into cliff face. Photos: Klath 2015.

Tml, lower Miocene. Primarily a calcareous unit (Figure 12). Well bedded (10-40cm thick). Dark brown/gray/tan on fresh surfaces with weathered surfaces appearing lighter white to tan. Fossil and fossil fragment rich. Strong reaction in >90% of beds tested to dilute HCl. ~5% occurrence of dolomite beds intermixed with shale/mudstone. Infilling of dolomite in shale/mudstone beds that are cracked is abundant. Oxidation staining from tar seeps present. Unit thickness averages 20m. Unit fails in large blocks creating daylighting beds and pocket beaches. Presence of active seeps, beach rock concretions, and tufa mineralization noted.

Figure 12. Images of lower Monterey, Shoreline Park, Santa Barbara Ca. Backpack and 30 cm bucket for scale (circled). Left: Head scarp of recent landslide activity visible by top of cliff. Right: groundwater seeps and tufa concretions on sea cliff face. Photos: Klath 2015.

Aerial Photo Annotation Analysis

Color aerial photographs provided by the 2013 California Coastal Records Project were compiled, printed on 8.5x11 sheets of paper, annotated in the field, and digitized using ArcGIS (v.10.2.2) upon completion of field surveying during the spring and summer of 2015 (Images 201308086 – 201308262). Images are available online through the California Coastal Records Project. Aerial photographs are useful in establishing previous landslide occurrences and the location of other notable features. In many cases, locations of features were visible on the photographs and accurate location placements, while also consulting Google Earth, were possible. However, the photographs relative scales are difficult to determine; they are not spatially or temporally consistent enough for incorporation into a statistical analysis program, e.g. – such as ArcGIS, and the oblique view to the earth at which they are taken makes establishing a scale difficult. Therefore manual entry of features into ArcGIS was required using annotated photographs and Google Earth.

Field Inventory: Sea cliff characteristics

Inventory items noted on aerial photos while field mapping include: active landslides visible along the field area >100m^3, active visible groundwater seepage from the cliffs, occurrences of tufa concretions and beach rock formations, drainage pipes inserted into or overlain onto the sea cliffs, beach access in the form of stairs or paths carved into the cliffs, homes close to the cliffs and visible support pilings exposed due to weathering, and fences constructed within or on top of the cliffs.

Digital Topographic Analysis

A bare earth, hydro flattened 1-m LiDAR DEM from the CA Coastal Conservancy LiDAR Project, flown from 2009-2011 (DOC/NOAA/NOS/OCM, 2012), was used to examine coastal cliffs and other features. The DEM is available at the National Oceanic and

Atmospheric Association (NOAA) Office for Coastal Management's (OCM) Data Access Viewer (Carignan et al., 2009). Using ArcGIS, corresponding landslide locations and other inventory items were manually placed on the DEM, aided by the use of Google Earth to improve precision. Within ArcGIS, corresponding, georectified, 1:24000 topographic maps downloaded from the USGS website (USGS 2014), as well as a georectified geologic map published by Minor et al., 2009, were incorporated into the DEM layer properties and consulted during map preparation and placement of features. Sea cliff characteristics (e.g. – cliff height, average slope, area, length, topographic profile) were extracted from the 1-m DEM using the spatial analyst tools available within ArcGIS.

Landslide Volume Calculations

Minimum landslide volumes were established, measuring landslides mapped in the field, by calculating approximate volumes. After creating a polygon representative of the landslide area, points are placed along scarp edges visible on the DEM and an interpolated "before landslide event surface" is generated. This "before" surface is subsequently subtracted from the actual land surface represented by the DEM using a cut/fill action within the spatial analyst toolbox in ArcGIS (Figure 13). This enables the following constraints to be placed on landslide volume throughout the field area with landslides characterized as small ($<100m^3$), medium ($\sim2500m^3$) and large ($>20{,}000m^3$). Several landslide events within Shoreline park and Rock Falls along Campus Point were measured directly (using a tape measure and known pace) and were found to be within several m^3 of values obtained using the cut/fill method in ArcGIS. Landslide events $<100m^3$ are deemed statistically unimportant in this study as they may be included in with surrounding larger landslide events. All landslides with volumes $>100m^3$ are noted on the final inventory map. Due to the method relying on

older scarp features within the DEM, these volumes are approximations of minimum values and may differ from actual values in the future.

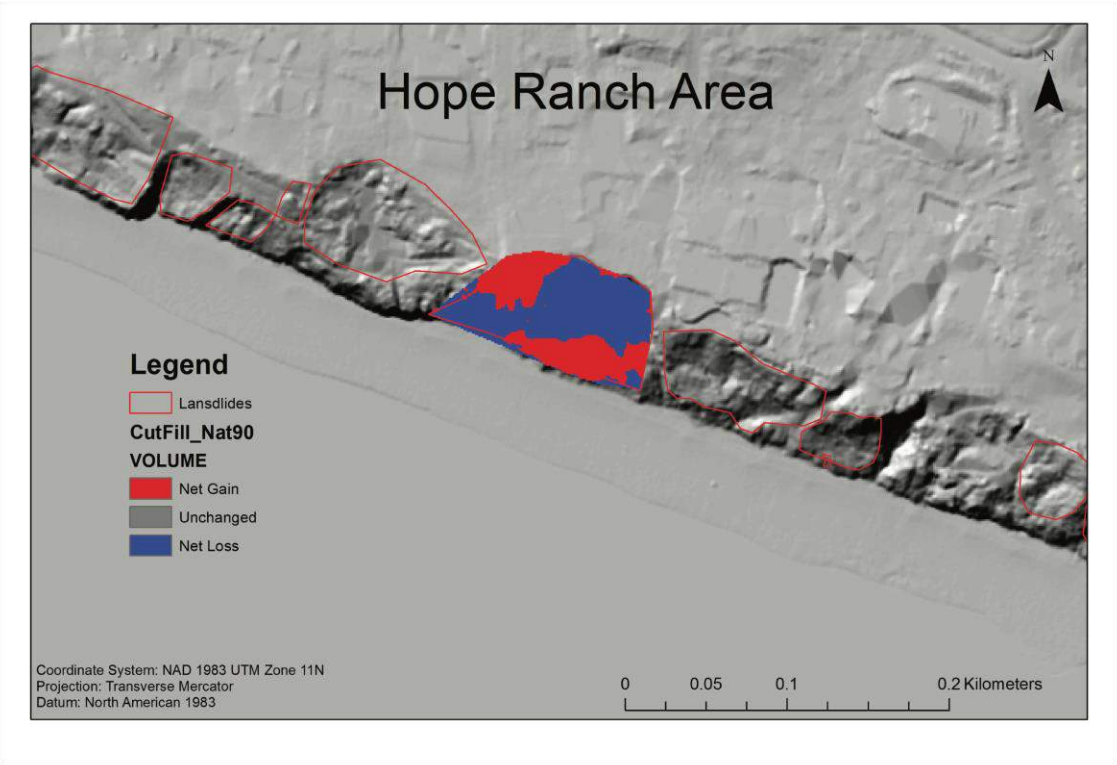

Figure 13. ArcGIS DEM landslide volume calculation. The pixels representing net loss are added together to obtain the total void volume between the before and after landslide event surfaces. Net gain pixels may be significant in that they potentially represent additional post landslide erosional surfaces but are not included in the final landslide volume calculated.

Schmidt Hammer

Bedrock rock strength was measured at each landslide, where possible, using a Schmidt hammer. The rebound values that are returned at each measurement site can be used as a relative means of comparing the hardness of different rock units. Due to the high variability of the Monterey formation, values may vary significantly from one location to

another, or even within exposed bedrock at a single landslide. 20-30 measurements were taken on multiple surfaces along each landslide. As with previous studies (Katz et al., 2000; Duvall et al., 2004; Keller et al., 2015), return values <10 and those that fractured the bedrock were rejected.

Analysis of Sea Cliff Variables

In order to evaluate whether rock type and other physical characteristics affect sea cliff failure volume and frequency, several statistical tests were employed to determine possible differences between units of the Monterey and Sisquoc shales. Landslide characteristics that were measured and tested include volume of failure, area of failure, sea cliff height associated with failure, rock competency, and bedding dip on or near a failure. Due to the small yet frequent nature of failure within section 5 (Tsq), landslides within this section do not meet the requisite >100m^3 minimum volume and are therefore omitted from most data analysis methods.

Using Matlab's correlation matrix function, an analysis of non-numerical data, also referred to as categorical data, such as the location of drainage pipes, stairs, seeps, etc…, was also completed. This method allows for a visual analysis to be done between individual section's categorical data.

Statistical Methods

Tests were implemented based on overall distribution patterns. First, testing for normality allowed for establishing whether parametric or non-parametric testing would be appropriate. Non-Parametric methods were used due to the non-gaussian nature of the data

distributions. Additional testing using paired testing methods allowed for the exploration of further statistical significance between rock units to be elucidated.

Kolmogorov Test (KS) for Normality

Landslide characteristics were tested for normality utilizing a single KS normality test. This test generates a p-value at the 2σ significance level. If the p value is < 0.05, the data set rejects the null hypothesis that the data is normally distributed and is determined to be non-normally distributed. Due to the dependence of this method on sample size, the data was also plotted in Matlab using the histogram function. It was determined, due to all data yielding non-gaussian distributions, that non-parametric tests would be most suitable when testing failure characteristics against rock type and one another.

Kruskal-Wallis Test

Kruskal-Wallis is a rank based, non-parametric test for determining if samples derive from similar distributions (Marsaglia et al, 2003; Alhakim and Hooper, 2008). This test allows for the comparison of more than two independent groups against a dependent variable and yields a p value and mean scores, at the 2σ significance level, which determines whether groups are significantly statistically different. This method is valuable in that it allows for the median and mean rank of the dependent variable (rock type) and independent variables (landslide characteristics) to be evaluated, helping to determine if there is a statistical difference within landslide characteristics between rock units. The outcome of this test is acceptance or rejection of the null hypothesis, where the null hypothesis states that the median or mean ranks are equal or not equal.

A critical assumption regarding the way null hypotheses are evaluated in using Kruskal Wallis concerns each datasets distribution. If the groups or pairs being tested have dissimilar distributions then mean ranks may be a more robust way to determine if datasets are different. Unequal mean ranks are indicative of data sets being significantly statistically different. Conclusions regarding differences in the median values for each group may only be made when population distributions are identical, data for both mean ranks and population medians with accompanying p values are also included.

Kolmogorov-Smirnov test (K-S test)

Due to distribution variations within the datasets and non-gaussian distributions, a K-S test was employed not only to test data distribution but also to determine statistical significance between datasets. K-S is a non-parametric, distribution independent method for measuring the probability that two datasets originate from the same population (Alhakim and Hooper, 2008; Marsaglia et al, 2003). This method allows for paired tests between independent variables and the dependent variable to be performed yielding a p value and k statistic (k-stat) at the 2σ significance level. K-stat values indicate the Δy (vertical y-axis difference) between two datasets; the larger the k-stat, the greater the difference between them. Paired testing allows for statistical differences to be elucidated further than by only using a Kruskal Wallis test for the entire sample characteristic population.

RESULTS

Data

All landslide data is compiled in Table 1. All landslide characteristics listed for each landslide are based upon the characteristics of each location and are not necessarily reflective of the area as a whole.

Table 1. Landslide Data for each mapped location >100m^3. 'SH' refers to Schmidt hammer readings along the base or toe (where available) of each landslide. 'Along reach' refers to the distance along the field area starting at Santa Barbara Point (0 km) to the east end of Goleta Beach (10.8 km).

LS #	LS Vol	LS Area	Rock Type	Type	SH	Dip□	Cliff Ht (m)	Along Reach (km)	Lat	Long
1	1497	314	Tml	trans block	31	40	15	0.2	34.3974	-119.7038
2	174	148	Tml	trans block	25	45	16	0.2	34.3971	-119.7044
3	130	62	Tml	wedge trans	20	45	16	0.3	34.3969	-119.7049
4	2472	488	Tml	rot trans block	18	33	16	0.3	34.3968	-119.7052
5	846	216	Tml	rot trans block	21	30	17	0.4	34.3966	-119.7061
6	117	75	Tml	wedge trans	27	35	20	0.9	34.3957	-119.7089
7	211	145	Tml	wedge trans	16	-20	22	0.9	34.3958	-119.7112
8	250	454	Tml	wedge trans	10	-20	24	1	34.3958	-119.7122
9	161	101	Tml	trans block	14	59	33	1.4	34.3962	-119.7170
10	2318	459	Tml	wedge trans	16	-64	34	1.5	34.3962	-119.7174
11	220	197	Tml	wedge trans	14	-25	39	1.6	34.3964	-119.7192
12	2331	1391	Tml	translation	0	55	36	1.9	34.3961	-119.7220
13	277	187	Tml	wedge trans	19	38	26	1.9	34.3957	-119.7235
14	47876	14586	Tmm	rot trans	30	34	39	2.2	34.3961	-119.7254
15	11200	4570	Tmm	rot trans	0	38	33	2.6	34.3966	-119.7293
16	5734	3717	Tmm	rot trans	0	17	43	2.8	34.3975	-119.7311
17	2088	770	Tmm	wedge trans	15	15	45	2.9	34.3976	-119.7318
18	3111	2420	Tmm	translation	15	45	47	3.1	34.3988	-119.7344
19	685	760	Tmm	rot trans	30	-37	47	3.2	34.3992	-119.7352
20	1249	822	Tmm	translation	20	-37	47	3.4	34.3994	-119.7357
21	8507	5520	Tmm	rot trans	26.4	50	48	3.5	34.3997	-119.7366
22	372	263	Tmm	translation	35	30	48	3.6	34.4004	-119.7379
23	523	701	Tmm	rot trans	35	30	48	3.7	34.4010	-119.7389
24	475	485	Tmm	translation	35	30	47	3.7	34.4016	-119.7395
25	252	475	Tmm	translation	35	54	46	3.8	34.4017	-119.7398
26	385	677	Tmm	translation	35	54	46	3.9	34.4023	-119.7411
27	128	272	Tmm	translation	31.6	41	46	4	34.4027	-119.7420
28	145	157	Tmm	wedge trans	12	58	46	4.3	34.4035	-119.7451
29	203	368	Tmm	translation	10.2	51	46	4.4	34.4038	-119.7465
30	12623	8943	Tmm	rot trans	0	24	48	4.5	34.4046	-119.7481
31	2115	1612	Tmm	translation	0	15	51	4.6	34.4044	-119.7494
32	3959	2458	Tmm	translation	10.4	15	52	4.8	34.4045	-119.7504
33	1128	487	Tmm	translation	0	45	52	5.3	34.4059	-119.7546
34	1002	353	Tmm	translation	0	45	52	5.4	34.4060	-119.7549
35	6697	2718	Tmm	rot trans	0	38	45	5.5	34.4073	-119.7580
36	4213	367	Tmm	translation	15	37	46	5.9	34.4086	-119.7618
37	423	633	Tmm	translation	11.8	38	41	6	34.4088	-119.7623
38	2273	1330	Tmm	translation	0	37	41	6	34.4090	-119.7627
39	2554	1252	Tmm	rot trans	10	38	40	6.1	34.4091	-119.7631
40	788	724	Tmm	rot trans	0	38	42	6.1	34.4092	-119.7635
41	1501	1006	Tmm	rot trans	11.7	33	41	6.2	34.4095	-119.7648
42	4809	2756	Tmm	rot trans	37.5	33	42	6.3	34.4098	-119.7658
43	18671	5449	Tmm	rot trans	0	12	45	6.4	34.4104	-119.7665
44	6555	3928	Tmm	translation	14.2	12	45	6.5	34.4106	-119.7679
45	577	538	Tmm	translation	0	48	44	6.7	34.4107	-119.7691
46	1472	954	Tmm	translation	22.7	48	43	6.7	34.4108	-119.7694
47	6218	2954	Tmm	translation	25.3	48	44	6.8	34.4111	-119.7704
48	124	343	Tmu	translation	27	50	40	6.9	34.4113	-119.7721
49	3955	2810	Tmu	translation	0	64	40	7	34.4119	-119.7730
50	271	227	Tmu	trans block	23.3	52	41	7.2	34.4129	-119.7750
51	415	432	Tmu	translation	10	52	41	7.3	34.4130	-119.7752
52	3042	1427	Tmu	wedge trans	0	49	42	7.4	34.4134	-119.7761
53	1500	1000	Tmu	translation	0	49	41	7.4	34.4135	-119.7764
54	308	389	Tmu	translation	0	57	39	7.8	34.4150	-119.7804
55	232	328	Tmu	translation	0	52	39	7.8	34.4153	-119.7810
56	224	369	Tmu	translation	0	52	41	7.9	34.4157	-119.7817
57	606	503	Tmu	translation	18	55	40	8.3	34.4166	-119.7850
58	581	540	Tsq	wedge trans	27	40	39	8.4	34.4168	-119.7856
59	1913	1143	Tsq	translation	0	32	39	8.5	34.4172	-119.7868
60	160	398	Tsq	translation	10.7	35	40	8.6	34.4177	-119.7889
61	425	386	Tsq	rot trans	0	35	39	8.7	34.4177	-119.7894
62	766	520	Tsq	rot trans	0	35	38	8.7	34.4177	-119.7897
63	1662	1069	Qcg	rot trans	0	-15	37	9.1	34.4184	-119.7941
64	864	426	Qss	wedge	0	-9	34	9.6	34.4183	-119.7997
65	443	328	Qss	wedge	0	-9	31	9.7	34.4184	-119.8001
66	1719	691	Qss	rot trans	0	-10	29	10	34.4185	-119.8037
67	499	641	QTst	debris fall	0	-11	27	10.5	34.4169	-119.8082
68	431	406	QTst	debris fall	0	-20	28	10.5	34.4168	-119.8100
69	760	601	QTst	debris fall	0	-20	26	10.6	34.4168	-119.8103
70	1537	932	Tsq	rot trans	0	-20	25	10.8	34.4171	-119.8117
*units in m3, m2, deg, or km			* negative dip indicates north dipping beds							

Landslide Inventory

Field work conducted through the spring, summer, and fall of 2015-2016, data collection, and recording of sea cliff variable observations have resulted in a comprehensive set of sea cliff variable data, multiple statistical comparison results between rock types/sections, detailed results for each landslide and their physical characteristics, and a comprehensive accounting of non-numerical data from the resulting human activity and development along the sea cliffs.

Table 2 reports details and results for each section. The average volume of failures within section 2 is greater than all other sections combined, as is the average volume of a single landslide. However, considering the length of section 2 versus the other sections, the number of failures per kilometer is not dissimilar from sections 1 and 3.

Bedding dip direction is variable throughout the field area among the abundant folds and changes in bedding orientation. Dominant dip direction is south for sections 1-3 but changes to north within section 4 along More Mesa. Section 4, with its deviation in bedding dip also notably has the lowest occurrence of failures per km as well as the lowest Schmidt hammer values.

Sections 2 and 3 have the highest cliff heights. This primarily due to high local uplift rates along these sections of sea cliff, as mentioned previously. Average slope values are also reported and are steepest along sections 1, 3, and 4. High reported uplift rates coupled with physical slope characteristics along section 2 contributing to failure could be the reason for a lower overall slope.

Lastly, where bedding creates a dip slope condition (daylighting beds), the dominant landslide type is a translational slip with little to no rotational component. Sections 1 and 3 are prone to this type of failure. Variations in bedding orientation within section 2 yields observations of translational slides often with a significant rotational component. Perhaps this is due to bedding being enabled to weather *in situ*, undisturbed for longer periods than those beds dipping steeply south acted more aggressively upon by gravitational forces.

Table 2. Landslide inventory, by section, along field area.

	Section 1	***Section 2***	***Section 3***	***Section 4***	***Section 5***
Section Length (km)	2	4.8	1.4	2.8	5.9
Total Failures	13	34	10	13	n/a
Total Failure Volume	11004	160511	10677	11760	n/a
Average Volume (m3)	846	4721	1068	905	n/a
Average Area (m2)	346	2207	783	622	n/a
Average Hardness (Base)	19	15	8	3	17
Failures/km	6.5	7.1	7	4.6	n/a
Average Cliff Height (m)	24	45	40	33	11
Average Slope	45°	35°	45°	43°	n/a
Dominant Dip Direction	South	South	South	North	North
Dominant Rock Type	Tml	Tmm	Tmu	Tsq/Qs	Tsq
Dominant Slide Type	translation	trans/rotation	translation	trans/rotation	debris fall

Further analysis of landslide characteristics was completed by evaluating the percent of each landslide type, orientation of bedding, and overall cliff height present within each section, Table 2. These results show:

1) the dominance of south dipping beds in sections 1, 2, and 3,

2) the highest percentage of failure occurs in sections with bedding dips >30°

3) translational landslides making up the majority failure type for sections 1 and 3,

4) the highest cliff heights within sections 2 and 3, also corresponds with localized more rapid uplift rates within the Santa Barbara coastal region,

5) and the total area of sea cliff versus the area of failure is the greatest within section 1.

Table 3. Percent of landslides corresponding with natural and cultural features.

For section 4: Where Sisquoc exposed, bedding dips SW or SE; Quaternary units all dip N to NE or NW. See appendix A for detailed geologic maps. Descriptions of calculation methods are below.

	Section 1	***Section 2***	***Section 3***	***Section 4***
Failure Vol/Area	2.2%	1.8%	2%	1.2%
Bedding Dip				
south	68%	90%	100%	38%
north	32%	10%	0%	62%
>30°	79%	66%	100%	33%
<30°	21%	34%	0%	66%
Landslide Type				
translation	85%	62%	100%	38%
rotate trans	15%	38%	0%	38%
debris fall	0%	0%	<1%	23%
Cliff Height				
cliff ht >30m	30%	100%	100%	62%
cliff ht<30m	69%	0%	0%	38%
Cultural Items				
Pipes	31%	44%	20%	15%
Seeps	46%	3%	0%	0%
Stairs/Fence	0%	41%	0%	38%

Bedding dip, landslide type, and cliff height percentages are out of 100% based on the occurrence of these characteristics within each section. Further analysis of landslide

inventory items includes landslide locations correlating to cultural features (Table 3). These percentages are found by dividing the total number of landslides in a section by the number of positive occurrences of a cultural feature on or by a landslide. Drainage pipes are most notable in sections 1 and 2 where 31% and 44% of the time pipes correspond to a landslide location. Seeps are most notable in section 1 through Shoreline Park where irrigation contributes to groundwater input. Stairs correspond to landslide locations 41% of the time in section 2 through Hope ranch. These are areas where homes above have direct access to the beach through the use of stairs built into the sea cliff. More detailed classification of drainage pipes is needed such as those hanging over cliff faces versus inserted into the cliffs. It should be noted that while not quantified in this study, most new, polyethylene pipes are draped over the sea cliffs while older, metal drainage is inserted into the sea cliff protruding out at the base. Pipes serve to drain excess precipitation and groundwater from the upper regions of sea cliffs and may only serve to highlight areas with higher population densities and subsequent development. The Hope Ranch development resides within sections 2 and 3 and areas along the sea cliffs with the greater number of pipes correspond to a greater number of houses above. It may be that due to the combination of a lower occurrence of drainage pipes within Shoreline Park and an observed increase in irrigation within the park, as compared to farther west; the likelihood of failure within the park is higher due to an increase of pore fluid pressure and a decrease in frictional forces between bedding planes (Blake et al, 2002).

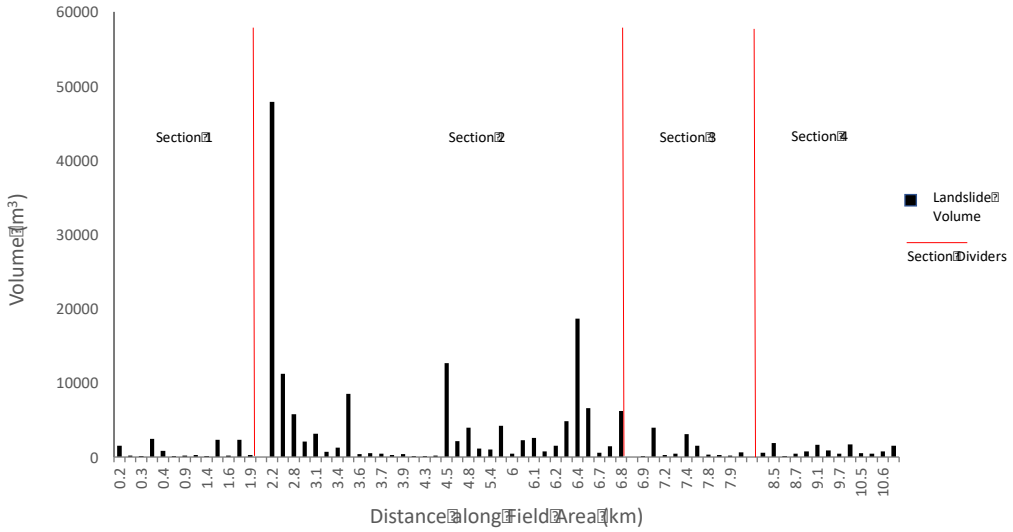

Figure 14. Landslide locations and volumes plotted with respect to distance along the field area. Distance begins 0 km at Santa Barbara Point running west to the eastern end of Goleta Beach at 10.6 km.

The most voluminous landslides, reside within sections 2 and 3 corresponding with the middle and upper Monterey units (Figure 14). These sections coincide with cliff heights >30m and south-southwesterly dip directions resulting in a dip slope condition. It should be noted that where shallower dips exist (<20º), bedding appears significantly more weathered than where steeper dips dominate.

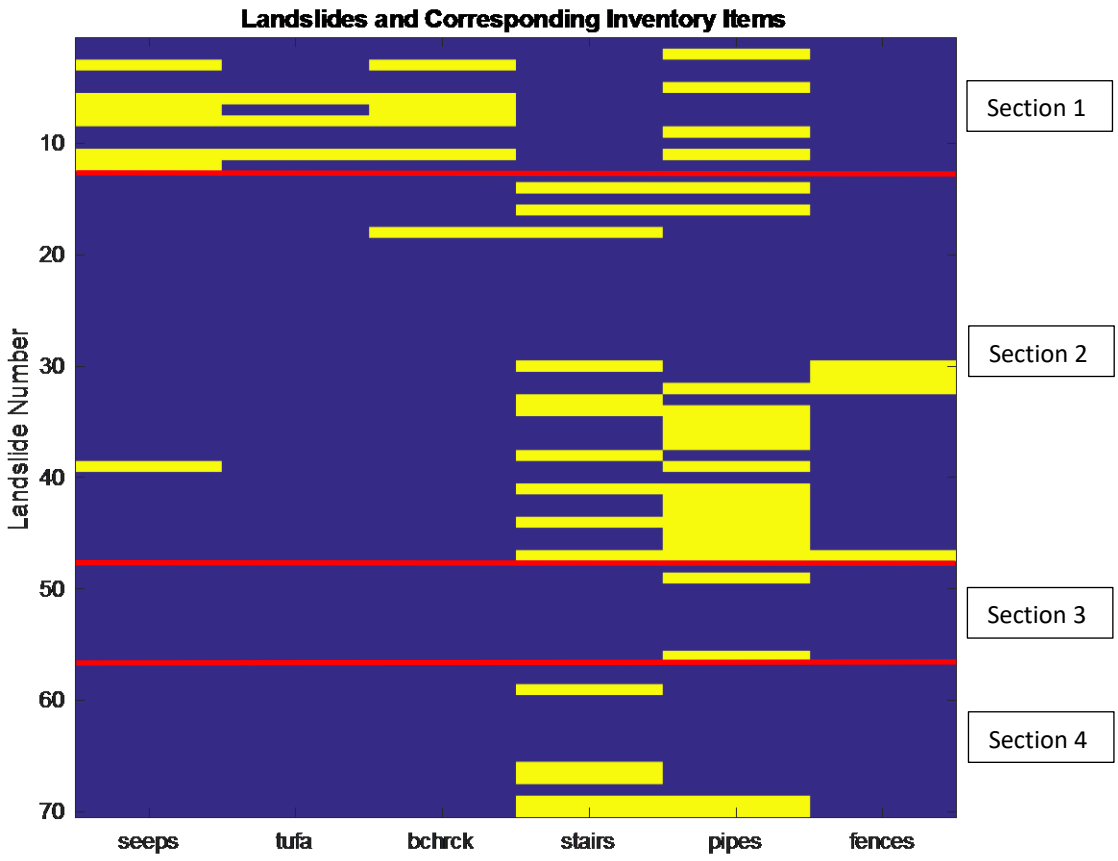

Figure 15. Correlation matrix and analysis of non-numerical data. Landslide numbers are on the y-axis (1-13 Tml, 14-47 Tmm, 48-56 Tmu, 57-70 Tsq/Qs), and categorical non-numerical inventory items are on the x-axis. Blue indicates no occurrence, yellow indicates a positive occurrence at a given landslide. 'Bchrck' indicates beachrock formations.

Key categorical data are included and show that where groundwater seepage is present, tufa and beach rock concretions are also present. This appears almost exclusively within section 1 (Figure 15). Many landslides appears to correspond to a human based feature whether drainage, stairs, or fences. Additionally, landslides occurring independently of any of these additional features are void of development and/or correspond to county parks or nature preserves (such as the Douglas preserve and More Mesa).

Schmidt Hammer Data

Average Schmidt Hammer rebound values from the bases of cliffs, adjacent to or on landslides, where available, represent relative compressive strength (hardness) of each unit (Table 2). Due to the high petrologic and weathering variability present within each rock type, measurements taken >1m above cliff bases generally returned as <10. Values >10, with few exceptions, were obtained from sea cliff bases and no higher than 1m above the base. Where wave action has direct access to sea cliff bases, these rock units yield higher rebound values and appear less weathered and more wave polished, Figure 16.

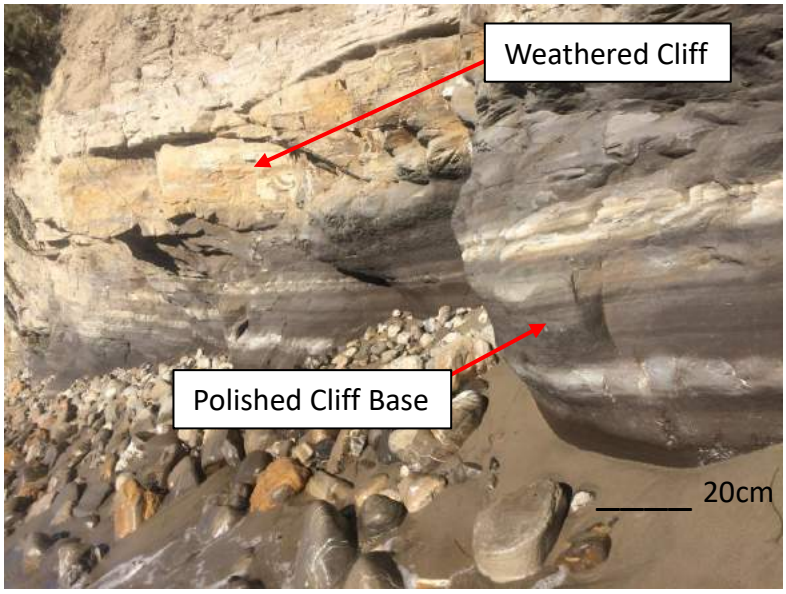

Figure 16. Image of Tml within Shoreline Park. Note polished, wave worn base and lighter, more weathered rock above where wave action has less access to rocks. Photo: Klath 2015.

Zero return values obtained at cliff bases are associated with wider beaches or rip rap placement in front of cliffs, infrequent wave access, and visibly higher degrees of weathering. Variations within hardness of weathered surfaces, among all rock types, range from 0 – 38. Figure 17 shows the range of rebound values within each section. Section 1

most notably yielded no non-zero return values. Section 2 shows the most variability with multiple <10 return values and others ranging the full gamut of 10-38. Most return values for sections 3 and 4 are <10 and section 5 returns either <10, or between 18-24. The results for section 3 (Tmu) were contrary to initial assessment as they were expected to return higher return values due to the dominant presence of siliceous phases than other units (e.g. – the less competent Sisquoc shale, or the visibly higher weathered calcareous/siliceous phased Tmm); these final results are contrary to initial assumptions and suggest that composition is not the primary driver behind return values. A second sampling of Tmu was taken from the sea cliffs along Goleta beach where the unit is significantly less weathered; rebound values are much higher through this part of the upper Monterey.

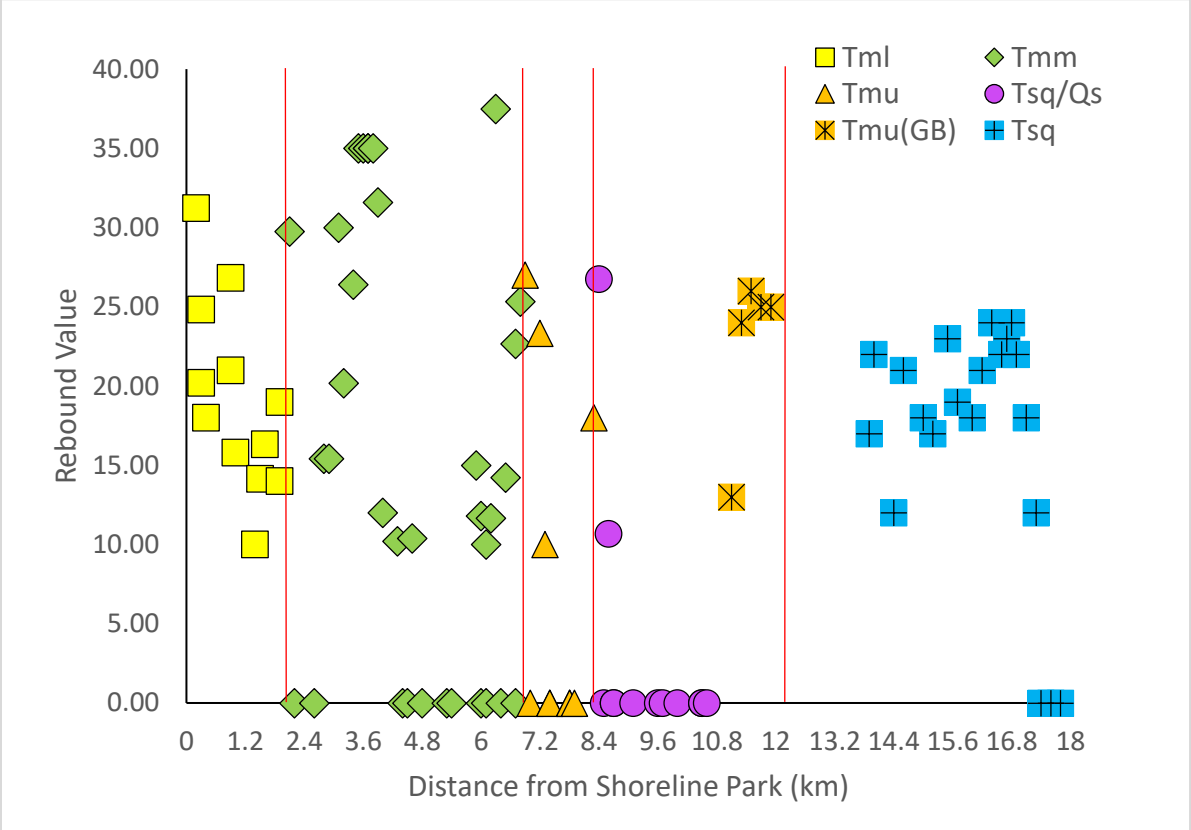

Figure 17. Schmidt hammer rebound values along the field area. Cliff base values are reported with other values collected vertically up section generally being discarded due to bedrock fracture or values <10 returned. Values correspond to landslides with the exception of Tsq and Tmu(GB) – upper Monterey along the Goleta Beach section where measurements were recorded every ~200 meters; Tmu along the Goleta Beach section are visibly less weathered and yield higher Schmidt hammer return values.

Cliff Top Sinuosity

To further quantify differences between each rock type, straight line distances were measured along the tops of sea cliffs for all sections. A second set of distances were collected that more carefully traced out each curve, bend, and twist of the cliff tops. These two numbers were divided together to create a sinuosity ratio, Table 4. Specifically:

$$\lambda = S_1/S_2 \qquad \text{(Equation 1)}$$

λ = Sinuosity ratio

S_1 = Actual, curved, cliff top distance

S_2 = Straight line cliff top distance

Table 4. Cliff top sinuosity distances and ratios for each section.

	S_1	S_2	$\boldsymbol{\lambda}$
Section 1 (Tml)	2388	2008	1.19
Section 2 (Tmm)	5124	4746	1.08
Section 3 (Tmu)	1516	1500	1.01
Section 4 (Tsq/Qs)	2793	2642	1.06
Section 5 (Tsq)	5017	4737	1.06


N
Shoreline Park Lower Monterey Sinuosity
FID Shape * Id length
0 Polyline 0 2388
1 Polyline 0 2008
Section 1 Length
Coordinate System: NAD 1983 UTM Zone 11N
Projection: Transverse Mercator
Datum: North American 1983
0 0.05 0.1 0.2 Kilometers

Figure 18. Section 1, Tml sinuosity measurement ratio results. Note the two distances obtained; a straight line measurement and a distance closely tracing the actual sea cliff top.

These results show:

1) the greatest sinuosity occurring in section 1. Section 1 is dominated by daylighting beds and resultant "pocket" beaches from cliff failure,
2) section 2, 4, and 5 have a less pronounced sinuosity but do show some variation,
3) and the 1.01 result from section 3 shows essentially no variation between straight line and actual cliff top distance. Referring back to Table 3, failure area % is high and steeply dipping beds dominate the reach suggesting that this unit fails in sheets – whole beds collapse in one failure event leaving little sinuosity on the remaining cliff face.

Sea Cliff Profile Analysis

Sea cliff profiles aid in determining dominant erosional processes at work on sea cliffs. Sea cliff profiles were generated using ArcGIS spatial analyst, obtaining x,y points along the vertical length of the cliff face. Measurements were obtained for each section, every 0.5 km. Referencing Figure 5, after Emory and Kuhn 1982, it is possible to analyze each sections profiles and determine the dominant erosional process at work within each section. M = marine and SA = terrestrial. Where profile numbers are omitted they are generally outliers, unrepresentative of a given section due to overdevelopment and/or abrupt change in geology/topography (e.g. – transition from anticline to syncline). Several profiles

at the west end of Goleta Beach and by Coal Oil Point were removed due to alternating fold structures from anticlinal to synclinal expressions yielding no change in elevation thus no profile. Figures 19 – 23 show each sections sea cliff profiles, beginning with section 1. Measurements were taken in ArcGIS using the spatial analyst tools and in 0.5km intervals along the reach. All profiles are shown with the same vertical and horizontal scales.

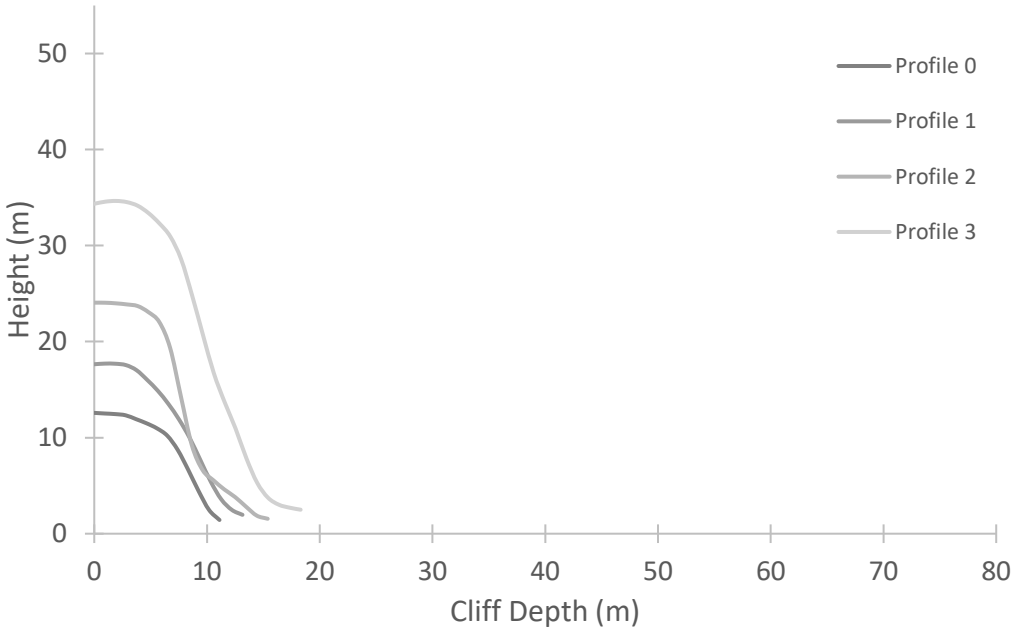

Figure 19. Sea cliff profiles for section 1.

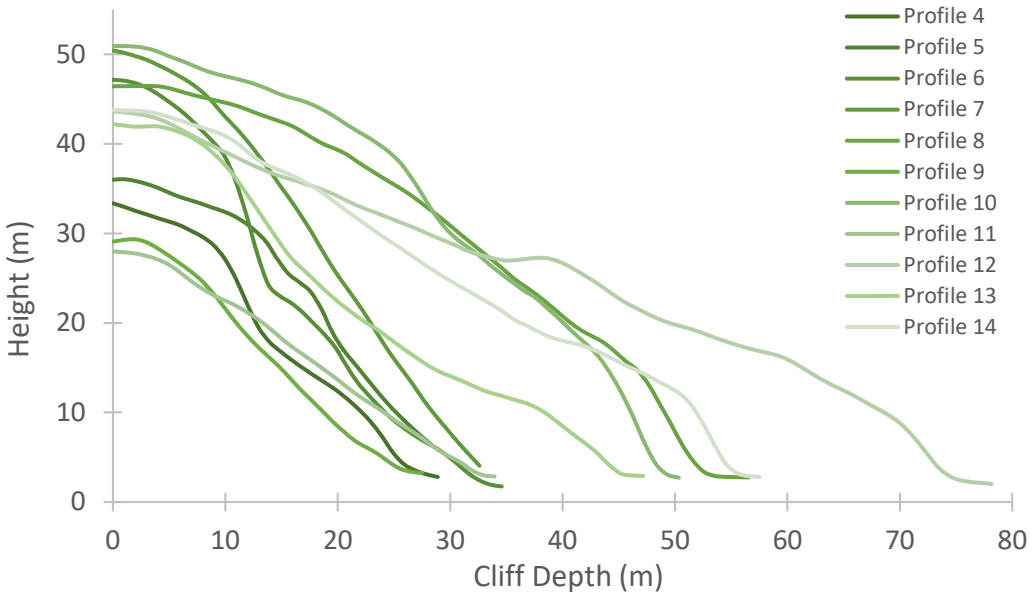

Figure 20. Sea cliff profiles for section 2.

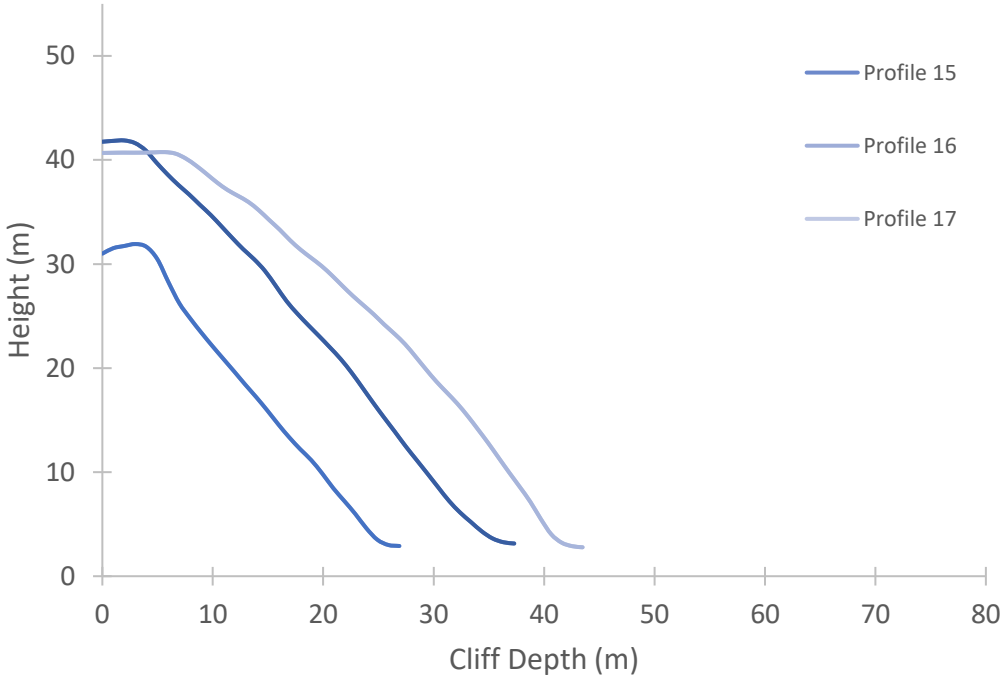

Figure 21. Sea cliff profiles for section 3.

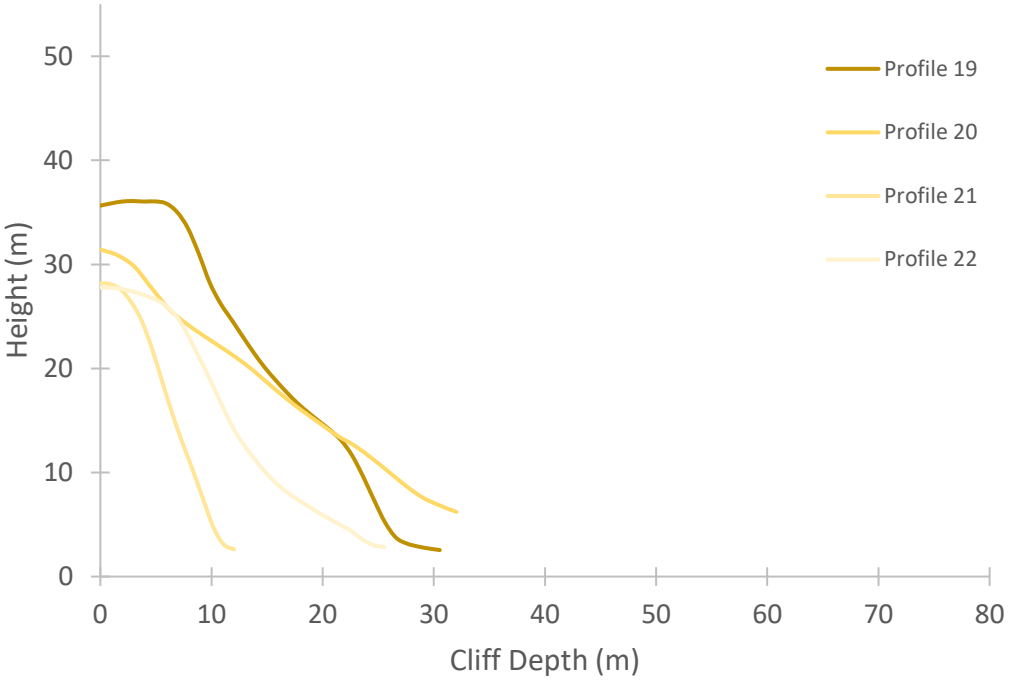

Figure 22. Sea cliff profiles for section 4.

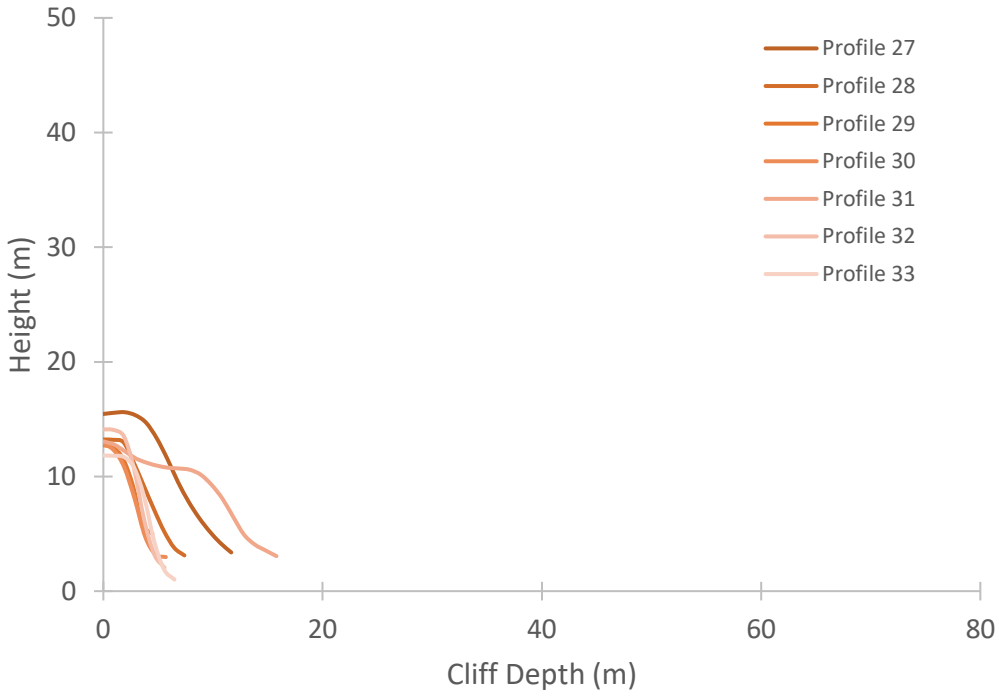

Figure 23. Sea cliff profiles for section 5.

Results show that:

1) Section 1 profiles indicate M ≥ SA and a shallow profile depth of <20 meters (x-axis).
2) Section 2 profiles are varied and extend in depth from east to west along section; overall, profiles reveal M ≤ SA, more often than M < SA,
3) Section 3 profiles show M < SA extending in depth east to west,
4) Section 4 varies with eastern areas expressing M ≥ SA and the western end M < SA, with a decrease in depth from east to west,
5) Section 5 overwhelmingly shows M > SA with a few exceptions where M ≥ SA and a depth generally ≤ 10 meters.

Overall, sections 2 and 3 experience greater terrestrial weathering than marine. It may also be inferred that due to the x-axis length of these profiles, the beaches are wider than in sections 1, 4, and 5. This idea is supported through observations made while field mapping. Areas with a smaller x-axis length were difficult to access except at minimum low tide. Sections 1, 4, and 5 profiles are indicative of cliffs undergoing either marine based or a combination of marine and sub-aerial based weathering processes.

Landslide Statistics

Distributions of Landslide Characteristics

Tests were performed on all the landslide data within a given characteristic to better understand overall distributions. These results are found in Figure 24 and Table 5. Individual section characteristics were then tested and results can be found in Figures 25-29 and Table

6. Results show all of the data are best described by non-gaussian distributions. Testing for data distributions is critical in moving forward with further statistical analysis as many tests are distribution dependent.

Figure 24 below show the results of simple frequency distributions. Each landslide characteristic, volume, area, hardness bedding dip, and cliff height, is evaluated to determine overall distribution patterns; all data are shown to have non-gaussian distributions. The log normal nature of the data are evaluated further by running each data set through a Kolmogorov-Smirnov calculator resulting in a p-value used to establish whether data comply with normal or non-normal distributions, Table 5.

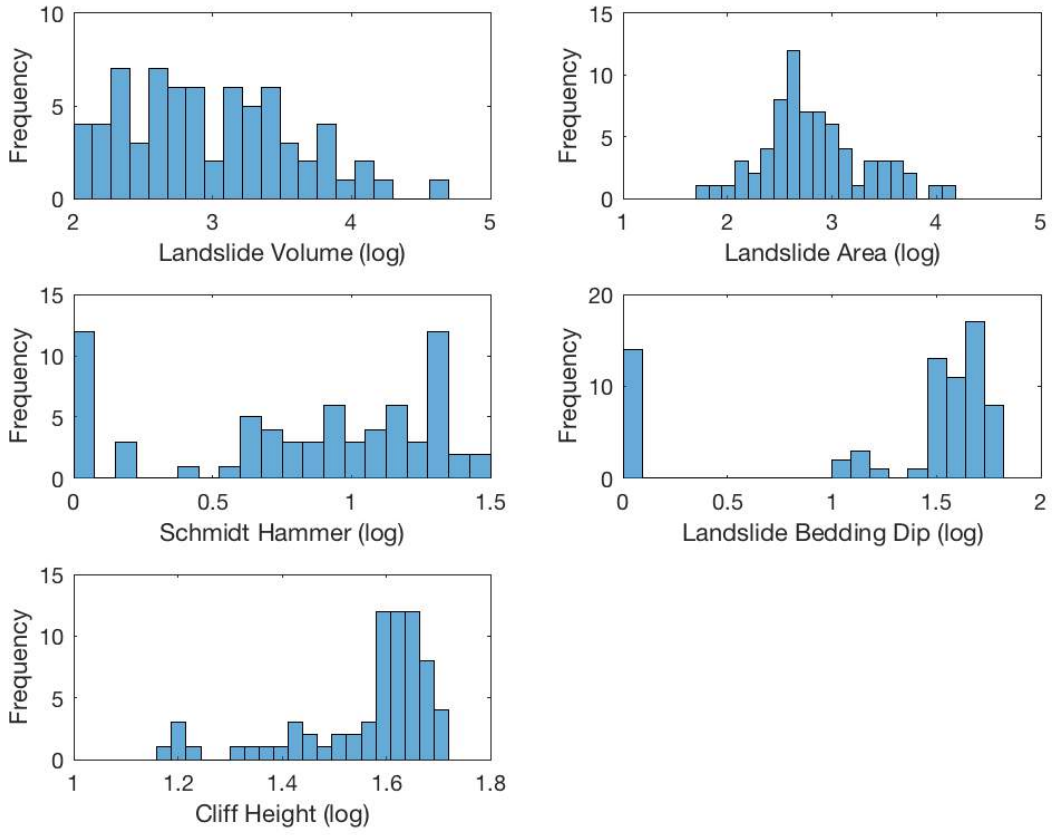

Figure 24. Distributions of landslide variables for all sections.

Table 5. Kolmogorov-Smirnov normality test results: p values < 0.05 reject the null hypotheses. Volume and Area numbers are higher for a log-normal distribution but do show a slight affinity for a normal distribution. All other characteristics cannot be described by standard distribution patterns.

	p (normal)	p (log-normal)	Distribution
Volume	0.11	0.7	log-normal
Area	0.12	0.38	log-normal
Hardness	0	0	0
Bedding Dip	0	0	0
Cliff Height	0	0	0

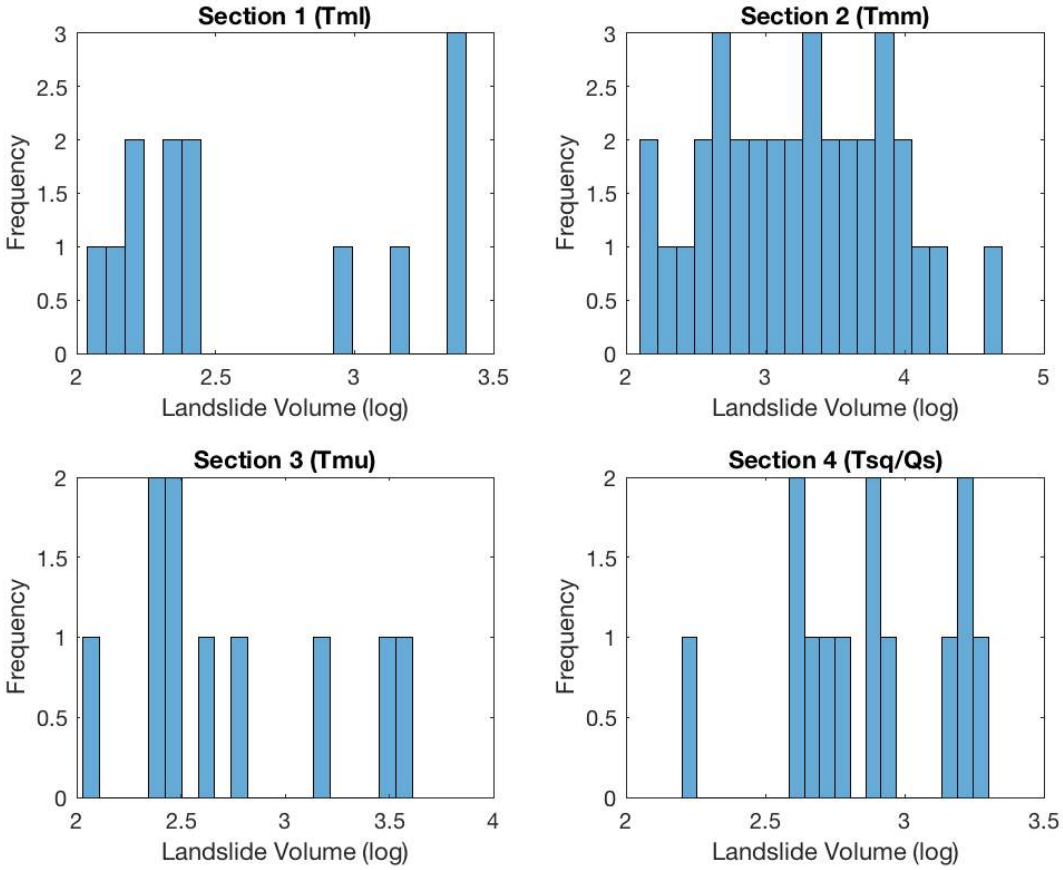

Figure 25. Distribution of landslide volumes with each section plotted individually.

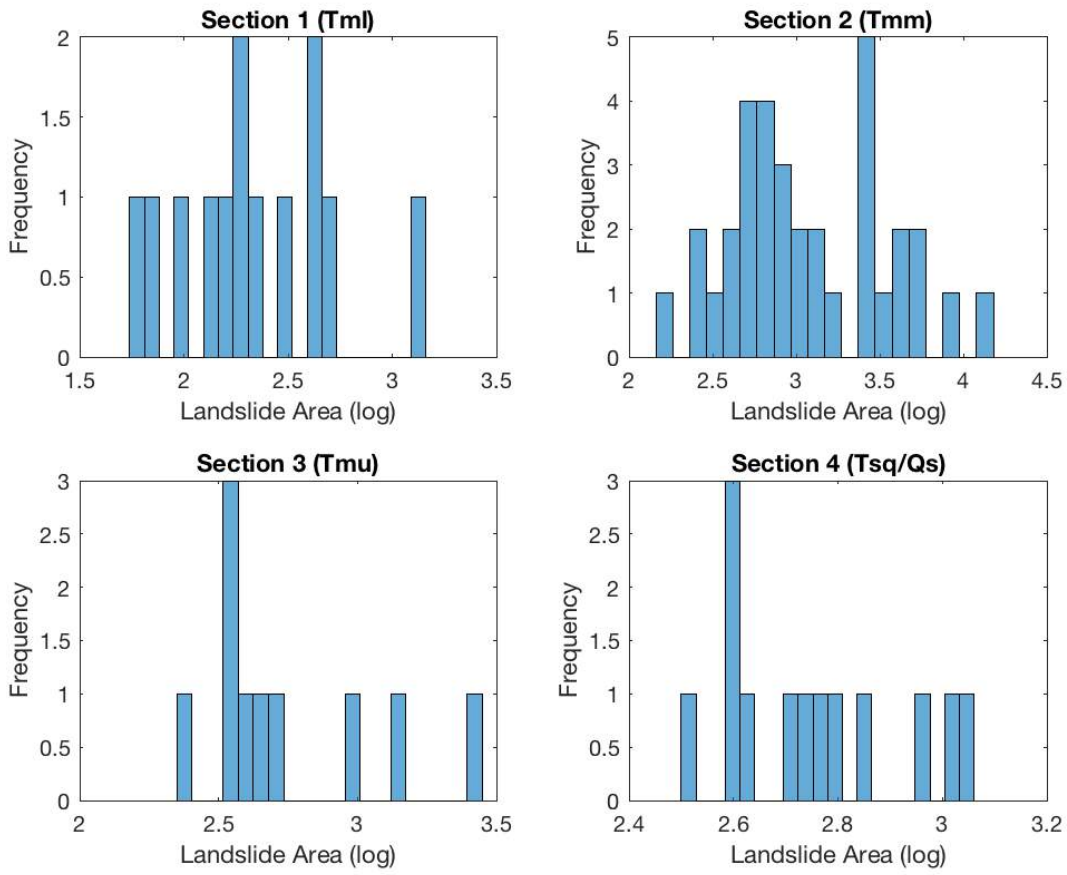

Figure 26. Distribution of landslide areas with each section plotted individually.

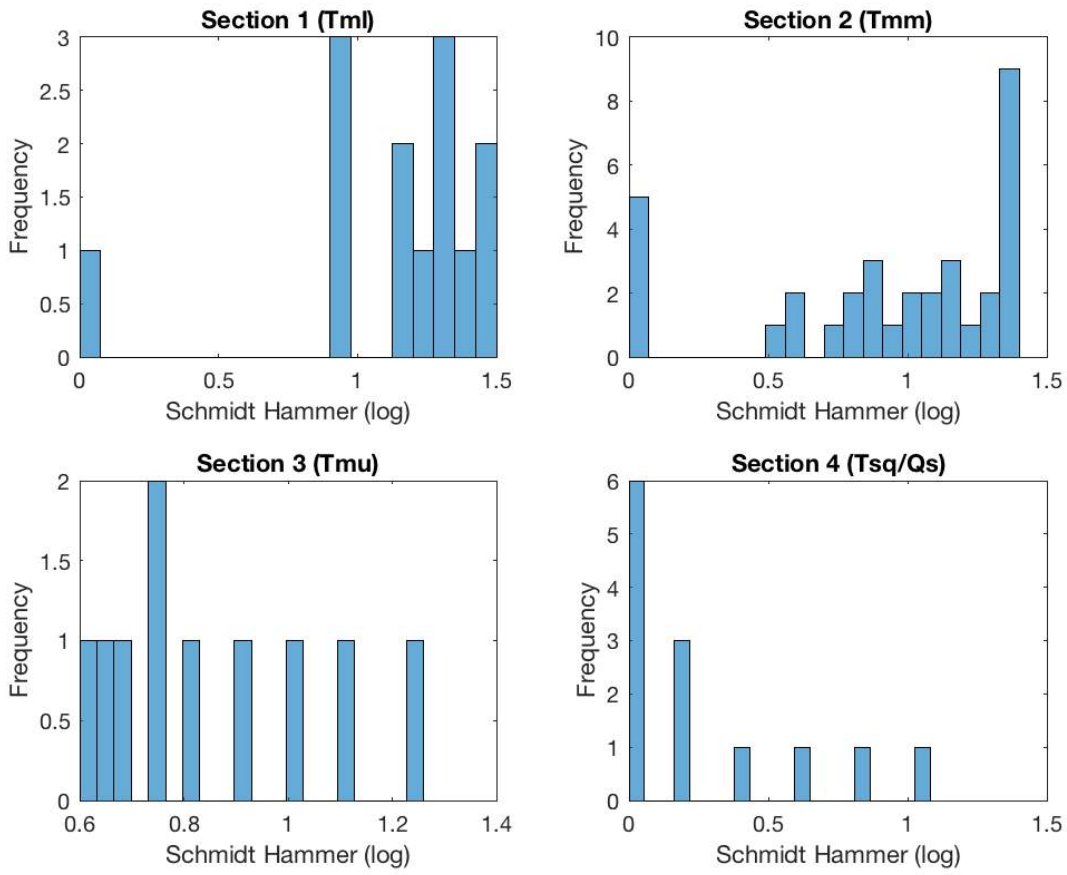

Figure 27. Distribution of Schmidt hammer values with each section plotted individually.

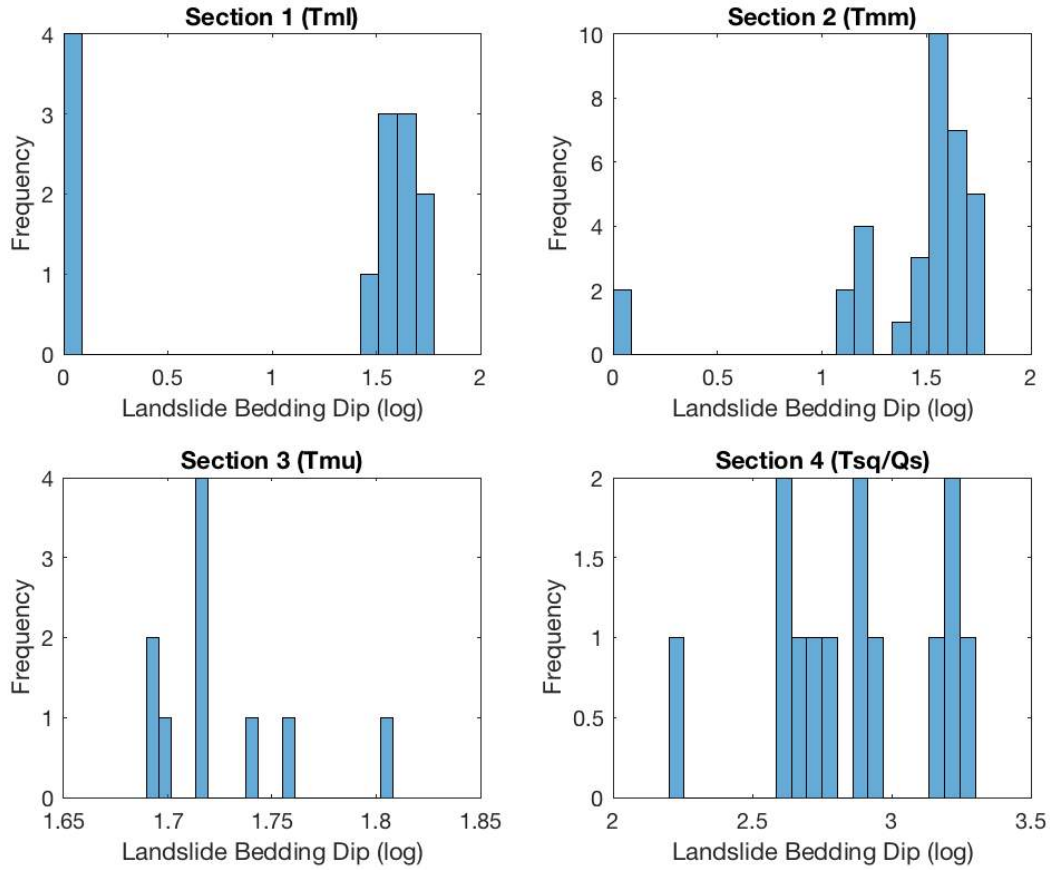

Figure 28. Distribution of bedding dip values with each section plotted individually.

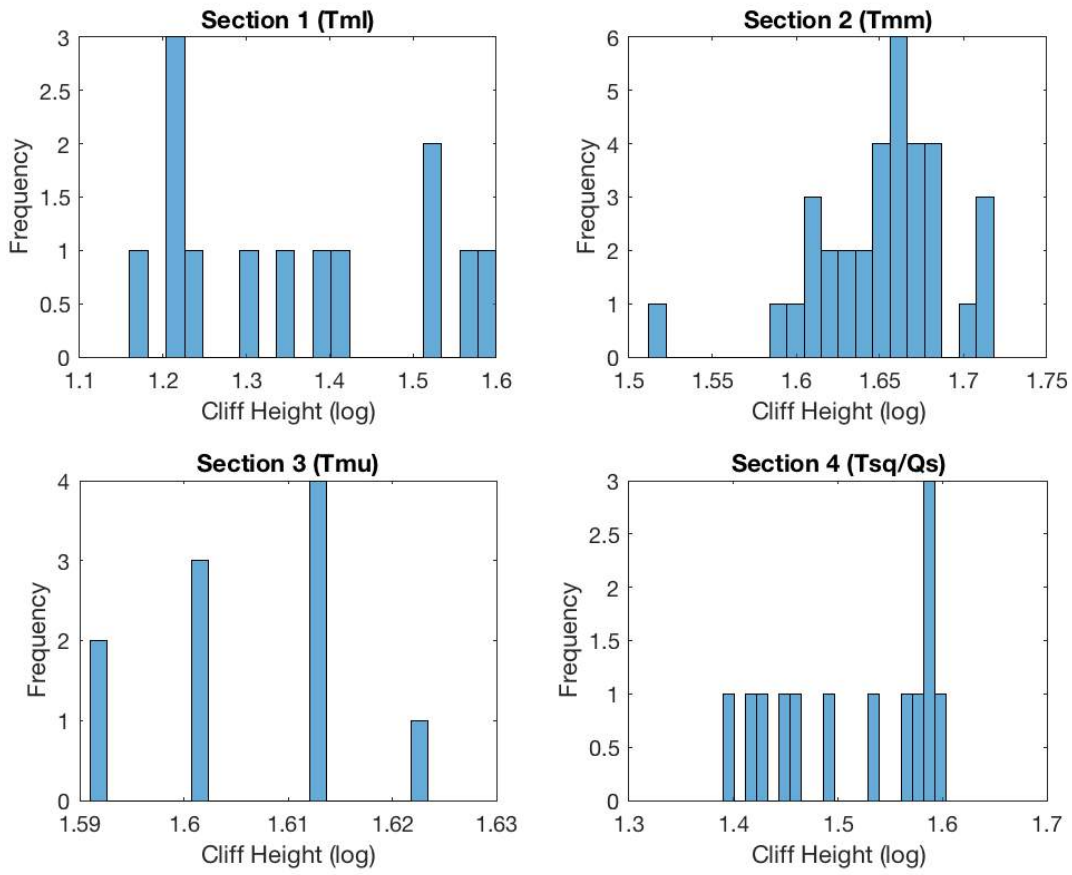

Figure 29. Distribution of cliff height values with each section plotted individually.

Table 6. Single Kolmogorov-Smirnov tests for normality.

All sections reject the null hypothesis that they derive from a normal distribution.

Volume	**p**	**result**
Section 1	0	reject
Section 2	0	reject
Section 3	0	reject
Section 4	0	reject
Area		
Section 1	0	reject
Section 2	0	reject
Section 3	0	reject
Section 4	0	reject
Hardness		
Section 1	0	reject
Section 2	0	reject
Section 3	0	reject
Section 4	0	reject
Bedding Dip		
Section 1	0.001	reject
Section 2	0	reject
Section 3	0	reject
Section 4	0	reject
Cliff Height		
Section 1	0	reject
Section 2	0.0016	reject
Section 3	0	reject
Section 4	0	reject

All data reject the null hypothesis that they derive from normal distributions, both within landslide characteristic whole datasets and individual section data. Moving forward with statistical analysis, it is clear that non-parametric testing is necessary.

Kruskal Wallis and Kolmogorov-Smirnov (K-S) Statistics

Kruskal Wallis results represent all sections tested together, for each variable, and calculates an R, chi-squared, a p value, and mean rank (Table 7). Differences in mean rank between sections and p values <005 indicate that they are unrelated and do not derive from similar distributions Each row within the table represents a variable; volume, area, hardness, bedding dip, and cliff height.

Table 7. Overall Kruskal Wallis test results.

Each landslide characteristic is divided into the four datasets representing each section/rock type; $p < 0.05$ and dissimilar mean ranks indicate rejection of the null hypothesis that the datasets are derived from similar distributions and medians.

	Mean Rank			
	Section 1	Section 2	Section 3	Section 4
Volume	24	43	27	33
Area	15	43	31	34
Hardness	43.5	39	27.5	19
Bedding Dip	32	34	60	19
Cliff Height	10	50	34	19
	R	**χ^2**	**p**	**result**
Volume	7.815	10.77	0.013	reject
Area	7.815	21.646	0.0001	reject
Hardness	7.815	21.646	0.0001	reject
Bedding Dip	7.815	24.167	0	reject
Cliff Height	7.815	51.259	0	reject

Kruskal Wallis results indicate, for all characteristics, the mean scores are not equal and p values reject the null hypothesis. Indicating that overall, within each landslide characteristic, none of the sections share similar values and are significantly statistically different from one another. Due to the rejection of the null hypothesis for each landslide characteristic, it

follows that individual paired tests within each variable be carried out to discover any further differences between rock groups.

K-S tests, Table 8, are the result of paired sections tested against one another and yield a p value and k-stat at the 2σ significance level. possible iterations for sections 1-4 were completed. Rejection of the null hypothesis indicates the sample means do not originate from the same distribution and that the groups are significantly statistically different. Additionally, to test for agreement with the null hypothesis, K-S identifies any deviation in median, variances, and distributions between groups. Due to this method testing for multiple deviations it is very powerful at detecting distribution shape changes but weaker at detecting median shifts (Lehmann, 2006). Statements regarding the acceptance or rejection of the null hypothesis and the size of k-stat value can only yield results that speak to whether or not a sample populations are similar/dissimilar and to what degree they may be similar or dissimilar.

K-S test results reveal that section 1, when compared with section 2, is different with respect to volume, area, or cliff height but shares similarities between hardness and bedding dip angle. Sections 1 and 3 are related with respect to volume and dissimilar considering area, hardness, bedding dip, and cliff height. Sections 1 and 4 share no similarities except for bedding dip direction. Comparing section 2 with section 3 shows they are similar in volume, area, and hardness values but have different distributions with respect to bedding dip and cliff height. Sections 2 and 4 are similar only in hardness values and differ in every other way. Finally, sections 3 and 4, like sections 2 and 3, reject cliff height and bedding dip but accept the null hypothesis for volume, area, and hardness.

Table 8. KS Test results, iterations for paired tests indicated by sections being compared, k-stat indicates the maximum (y value) difference between each section.

Volume		p	result	k stat
	Sections 1 & 2	0.0117	reject	0.4977
	Sections 1 & 3	0.3662	accept	0.3615
	Sections 1 & 4	0.028	reject	0.5385
	Sections 2 & 3	0.0901	accept	0.4235
	Sections 2 & 4	0.0111	reject	0.5
	Sections 3 & 4	0.058	accept	0.5231
Area				
	Sections 1 & 2	0.00018	reject	0.6697
	Sections 1 & 3	0.0149	reject	0.6154
	Sections 1 & 4	0.0017	reject	0.6923
	Sections 2 & 3	0.0757	accept	0.4353
	Sections 2 & 4	0.0351	reject	0.4412
	Sections 3 & 4	0.4202	accept	0.3462
Hardness				
	Sections 1 & 2	0.1068	accept	0.3756
	Sections 1 & 3	0.0421	reject	0.5462
	Sections 1 & 4	0.0017	reject	0.6923
	Sections 2 & 3	0.3479	accept	0/3176
	Sections 2 & 4	0.0547	accept	0.4163
	Sections 3 & 4	0.9042	accept	0.2231
Bedding Dip				
	Sections 1 & 2	0.5409	accept	0.2489
	Sections 1 & 3	0.00018	reject	0.8462
	Sections 1 & 4	0.2264	accept	0.3846
	Sections 2 & 3	0	reject	0.8529
	Sections 2 & 4	0.0032	reject	0.5566
	Sections 3 & 4	0	reject	1
Cliff Height				
	Sections 1 & 2	0	reject	0.9412
	Sections 1 & 3	0	reject	0.9231
	Sections 1 & 4	0.0076	reject	0.6154
	Sections 2 & 3	0	reject	0.7647
	Sections 2 & 4	0	reject	0.9118
	Sections 3 & 4	0.0023	reject	0.7231

DISCUSSION

Landslide Inventory Synthesis

In an effort to elucidate possible differences between sub units of the Monterey shale and between the Sisquoc shale, multiple quantitative and qualitative methods were employed. The overarching question of how rock type may influence the volume, style, and frequency of landsliding along the Santa Barbara coastline is explored and, when considering variation in rock type in conjunction with physical variables; bedding dip orientation, rock strength, and cliff height, as well as weathering mechanisms, individual units do display variations. While some units behave similarly, each unit displays varying and distinct weathering patterns as well as varied failure responses resultant from physical characteristics. The following discussion will focus on these differences between rock units and attempt to characterize each ones failure tendencies and overall expectations for future landsliding activities. Qualitative results, including field observations, and quantitative results are emphasized to distinguish each unit and fully characterize unit differences and behavior.

Physical variables driving sea cliff failure: a comparison

Rapid uplift rates, varying composition between units, and different weathering drivers all contribute to the varied landslide tendencies visible along the coastline. Sections 2 and 3 are affected by higher rates of local tectonic uplift and contain, per km, more instances of failure. Section 1, despite a lower average cliff height when compared to sections 2 and 3, experiences failure nearly similarly. This can be attributed to daylighting bedding conditions and highlights that in the absence of higher local tectonic uplift rates, failure is driven in part by other factors. Areas with average bedding dips >30^{o} are

characterized with a greater number of landslides, thus contributing to overall measurable higher landslide occurrence within section 1-3. The presence of daylighting beds, while contributing to higher landslide frequency, most notably within section 1 and 3, does not yield the most voluminous landslides. Section 2 is highly varied in both unit orientation and overall bedding composition and contains failures an order of magnitude larger than all other sections.

The largest landslides are present where bedding dip is not as pronounced. These areas of lower dip allow the unit to weather in situ for longer periods and parts of the middle Monterey (section 2) are so highly weathered they appear and behave more as a soil than a competent rock. High degrees of weathering coupled with high uplift rates within this section contribute to large, voluminous failure, as the rocks weather in place they lose competency and cease to behave as a single, coherent bed failing translationally, as with the lower and upper Monterey. Overall, this allows for more voluminous landslide events along the middle Monterey coastal section.

Weathering and overall rock competence also affects landslide style. Units that have experienced higher degrees of weathering yield different styles of failure. Sections 2 and 4, behaving more like a soil and containing higher degrees of weathering, tend to fail in a rotational translational way leaving behind a deep scar in the middle to upper sections of the sea cliffs. Failure is generally characterized from the sea cliff top in these highly weathered sections and failure does not necessarily affect the sea cliff base. Section 2 also contains steeply dipping beds that fail translationally and remove entire sections of sea cliff from base to top. This translational style effecting the entirety of the sea cliff profile is the most common behavior seen within sections 1 and 3 and results, most notably within

section 1, in distinctive geomorphology visible in form of ‘pocket beaches’.

Physical sea cliff variables and variations; geomorphology and petrology

The geomorphological changes that manifest as the result of landsliding on sea cliffs may be characterized by sea cliff profiles. The overall shape of a section of sea cliff can be indicative of the dominant weathering processes at work in that area. Sinuosity ratios may also serve as a way to visualize and characterize changes in and differences between rock types. Ratios were calculated for each section, Table 3, and it was found that the highest sinuosity ratio is within section 1, an area that experiences translational failure leaving visible scars along the sea cliff, thus highlighting the overall tendency for this unit to fail translationally due to the high occurrence of daylighting bedding conditions. Weathering mechanisms are explored after assigning each section, based on its overall profile, the dominant mechanism being categorized as marine and/or terrestrial, as described by Emory and Kuhn (Figure 5). Section 2 is acted upon more vigorously by terrestrial weathering and further explains the tendency towards rotational failure in the upper vertical reaches of the sea cliffs. Sections 1, 3, and 4 are acted upon in large part by both marine and terrestrial weathering leaving a moderately steep profile that enables more frequent landsliding; as failures occur at both top and base, ocean waves act to remove supporting toe materials from the sea cliff bases, and more failures, albeit less voluminous, are apparent. While structural features and resulting geomorphological changes in the sea cliffs may be explained by weathering processes and profiles, these changes may also be linked to rock type.

The lithology of each section may be linked to sea cliff failure behavior; mineral and

biological constituents within the shales contribute to the rate of weathering a given unit undergoes over time (Chigira and Oyama, 2000) thus effecting failure style and size. The lower and upper Monterey are both comprised of massively bedded siliceous and calcareous mudstone/shale that is more resistant to weathering than the more finely laminated, calcium based mineralogical constituents of the middle Monterey shale. All subunits do contain minor apatite, porcelanite, and chert, but overall, silica versus calcium based mineral constituents dominating a given unit has a clear impact on weathering (Minor et al., 2009).

Revisiting the stratigraphic column in Figure 12 and examining the sea cliff profiles in Figure 19, an attempt to quantify differences in the hardness of each unit and thus the degree of weathering, was implemented by testing each units compressive strength with a Schmidt hammer. Considering that differential weathering will cause multiple variable return readings within a single bed, average readings are examined. In conclusion, due to the variability of the return readings, Schmidt hammer values are likely a product of degree of weathering within a given unit and not necessarily a measure of unit competence.

Sisquoc Shale: Section 5 Discussion

Section 5, Tsq, is omitted from statistical testing and other tests performed on sections 1-4. Explained previously, measuring volume and area of failure within this section is difficult as there were, at the time of data collection, no failures that met the study criteria for volumes >100m^3. Overall, Section 5 has an average cliff height of 11m, the lowest of all sections. It does have some of the highest cliff slopes along the field area reach, 45º, and is

capped off by a distinctive layer of quaternary paleo dune sands that range from 1-4m thick. This unit occurs predominately within the UCSB campus and Isla Vista community and is highly developed within most of the field area. Non-native ice plant and other water rich succulents are noted within campus areas and around homes on the sea cliffs. Ice plant, beyond being decorative, is placed in areas to arrest erosion in soft rock but can have the added effect of increasing overburden weight to fragile sea cliffs, especially a compacted shale like the Sisquoc. Figure 30 highlights the highly developed nature of the sea cliffs within Isla Vista.

Figure 30. Section 5, Tsq. Isla Vista, Camino Pescadero Beach Access Stairs. Note exposed pillar supports, overhanging mat like vegetation, and people at cliff base for scale (1.75m). Photo: Klath 2015.

Considering the Sisquoc is a weaker compaction shale with average compressive strength values (above max tide lines where wave polished bases are exposed) of zero throughout with heavy sediments, vegetation, and development on top, as well as more rapid retreat rates

than other sections (Griggs et al., 2005), this area is at a high at risk for failure and negative economic impact for the Santa Barbara and UCSB communities.

Future Work

Several important topics directly impactful to this study should be further explored in order to obtain a more complete understanding of the Santa Barbara coastal region.

1) Archived aerial photo analysis of sea cliffs to better constrain landslide recurrence intervals and further quantify local retreat rates and the nature of failure between rock units. Several collections (Fairchild, Hurd), going back in some locations to the 1930s, are available for analysis.
2) Classification of groundwater seeps into irrigation based and rain runoff based to better understand flow/infiltration rates and the potential seasonality of both.
3) Classification of vegetation coverage and plant species along the sea cliffs. Many non-native, ornamental plant species grow on and above sea cliff surfaces. In many cases these plants add water and overburden to the cliffs possibly increasing the likelihood of failure in those areas. A better understanding of these areas can be added to an already comprehensive landslide inventory.
4) Classification of drainage pipes, in ground or above, and how many correspond to an active landslide area. Oftentimes the occurrence of drainage pipes at the bases of sea cliffs correlate to housing development above. They represent an effort to alleviate possible groundwater infiltration and increased overburden pressure on the cliffs. A better understanding of how well these pipes work would be important to future work in the area.

Conclusions

The main conclusions of this study are

1. The composition of bedding along the field area effects the style and extent of failure. Mineral constituents are key to understanding how quickly units will fail. Bedding more resistant to weathering has more visible Si rich interbeds and will resist rotational landsliding. However, translational slip may occur, especially in areas with greater human development and activity.

2. Structural features within the sea cliffs also effect the style and extent of failure. In areas with an existing dip slope condition, there are a greater number of landslides per unit length.

3. Schmidt hammer rebound values are not necessarily a measure of an individual rock units compressive strength, but more likely a measure of the degree of weathering in and around an individual landslide.

4. The presence of human activity and groundwater infiltration, natural or human based, will affect the rate of weathering on the sea cliffs.

References

Alhakim, A., Hooper, W., (2008). A non-parametric test for several independent samples, Journal of Nonparametric Statistics, 20:3, 253-261.

Bird, E., (2016). Coastal Cliffs: Morphology and Management. Springer Briefs in earth sciences.

Blake, T.F., Hollingsworth, R.A., Stewart, J.P., (2002). Recommended Procedures for the Implementation of DMG Special Publication 117: Guidelines for Analyzing and Mitigating Landslide hazards in California.

Blueford, J., Isaacs, C., Murchey, B. and Barron, J. (1989) Field Trip Guide to the Miocene Monterey Formation, Salinas and Santa Barbara Areas, California, in Mesozoic and Cenozoic Siliceous Sediments of California: San Francisco to Los Angeles, California, July 3-7, 1989, American Geophysical Union, Washington, D. C..

Carignan, K.S., Taylor, L.A., Eakins, B.W., Warnken, R.R., Lim, E., Medley, P.R., (2009). Digital Elevation Model of Santa Barbara, California: Procedures, data sources and analysis. NOAA Technical memorandum, NESDIS NGDC-29.

Chigira, M., Oyama, T., (2000). Mechanism and effect of chemical weathering of sedimentary rocks. Eng. Geol., Vol 55, Issues 1-2, pp 3-14.

Emory, K.O. and Kuhn, G.G., (1982). Sea Cliffs: Their processes, profiles, and classification. GSA bulletin, Vol 93 (644-65).

Griggs, G., Patsch, K., Savoy, L. (2005). With contributions by Reinhard Flick, Kim Fulton-Bennett, Karen Grove, Cheryl Hapke,Kenneth R. Lajoie, Charles F. Lester, Scott Mathieson, Dorothy Merritts, Robert M. Norris,Antony R. Orme, Bernard Pipkin, Derek Rust, Douglas Sherman, Robert Walker, Jerry Weber. Living with the Changing California coast. University of California Press, Edition 1.

Griggs, G., Russell, N., (2012). City of Santa Barbara sea-level rise vulnerability study. California Energy Commission, CEC-500-2012-039.

Gurrola, L.D., Keller, E.A., Chen, J.H., Owen, L.A., Spencer, J.Q., (2014). Tectonic Geomorphology of marine terraces: Santa Barbara fold belt, California. GSA Bulletin 2014, no.1-2;219-233.

Hampton, M.A., Griggs, G.B., (2004). Formation, Evolution, and Stability of Coastal cliffs – Status and Trends. USGS Professional paper 1693.

Hapke, C.J., Reid, D., Richmond, B., (2009). Rates and Trends of coastal change in California and the regional behavior of the beach and cliff system. Journal of Coastal Research, 25,3 (603-615).

Katz, O., Reches, Z., Roegiers, J.C., (2000). Evaluation of mechanical rock properties using a Schmidt Hammers. Int. J. Rock Mech. Min Sci. 37, 723-728.

Keller, E.A., Gurrola, L.D., (2000). U.S.G.S. National Earthquake Hazard Final report, July 2000, Earthquake hazard of the Santa Barbara Fold Belt, California. http://www.geol.ucsb.edu/~keller/sbeqh.pdf.

Keller, E.A., Duffy, M., Kennett, J.P., and Hill, T., (2007). Tectonic geomorphology of the Mid-Channel Anti-cline, Santa Barbara Basin, California: Geomorphology, v. 89, p. 274–286.

Keller, E.A, Bean, G., Best, D., (2015). Fluvial geomorphology of a boulder-bed, debris-flow — Dominated channel in an active tectonic environment. Geomorphology 243, 14-26.

Komar, P.D., (1998). Beach processes and sedimentation, 2nd Ed. Prentice Hall.

Lehmann, E.L., D'Abrera, H.J.M. (2006). Nonparametrics: Statistical methods based on ranks. 2nd edition. Springer science+business media. ISBN-10: 0-387-35212-0.

MacKinnon, T. C. (1989). Origin of the Miocene Monterey Formation in California, in Oil in the Monterey California Formation Los Angeles to Santa Maria, California July 20-24, 1989 (eds T. MacKinnon, J. W. Randall and R. E. Garrison), American Geophysical Union, Washington, D. C.. doi: 10.1029/FT311p0001.

Marsaglia, G., W. Tsang, and J. Wang. (2003). Evaluating Kolmogorov's Distribution. *Journal of Statistical Software*. Vol. 8, Issue 18.

Minor, S.A., Kellogg, K.S., Stanley, R.G., Gurrola, L.D.Keller, E.A., and Brandt, T.R., (2009) Geologic map of the Santa Barbara coastal plain area, Santa Barbara County, California: U.S. Geological Survey Special Investigations Map 3001. Scale 1:25,000.

Norris, R., Back, W., (1990). Erosion of seacliffs by groundwater. GSA Special paper 252.

Norris, R, (1990). Seacliff erosion: a major dilemma. California Geology, (171-177).

Parrish, J.G., (2008). Guidelines for Evaluating and Mitigating Seismic Hazards in California. California Geological Survey, Special publication 117A.

Sunamura, T., (2015). Rocky coast processes: with special reference to the recession of soft rock cliffs. Proc. Jpn. Acad., Ser. B 91.

Sylvester, A.G., (2016). UCSB Beach: 45 years of waxing and waning. http://www.geol.ucsb.edu/faculty/sylvester/UCSBbeaches.html.

USDA, 2012, Part 631 Geology, National Engineering Handbook: Chapter 4, Engineering Classification of Rock Materials. 210-VI-NEH, Amend. 55.

Van Asch, T. W., Buma, J., and Van Beek, L., 1999, A view on some hydrological triggering systems in landslides: Geomorphology, v. 30, no. 1, p. 25-32.

Young, A.P., Guza, R. T., O'Reilly, W.C., Flick, R.E., and Gutierrez, R., (2011). Short-term retreat statistics of a slowly eroding coastal cliff. Nat. Hazards Earth Syst. Sci., 11, 205–217, 201doi:10.5194/nhess-11-205-2011.

Appendix A. Detailed Geologic Maps of Field Area by Section

Red markers indicate mapped landslides.

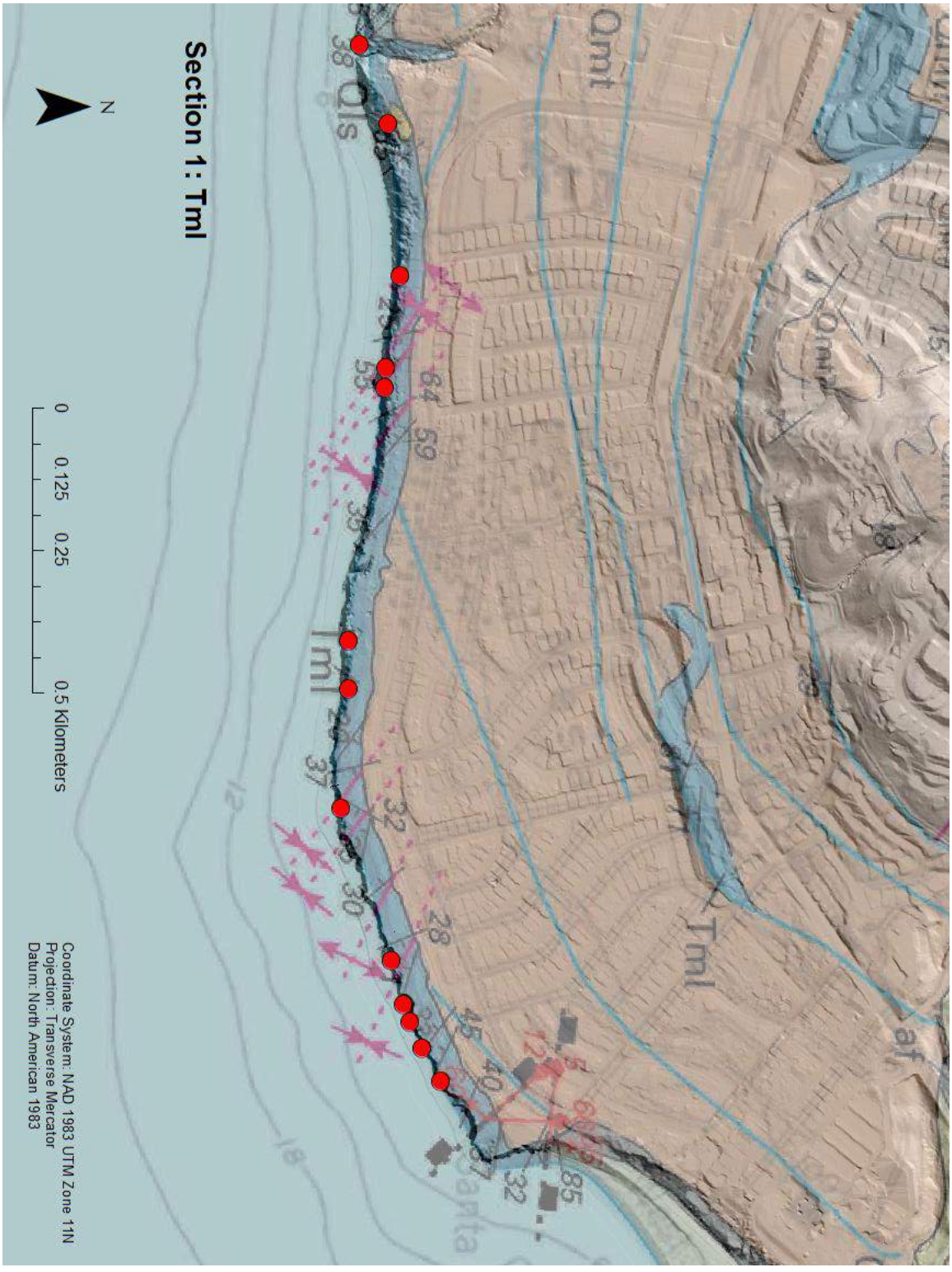

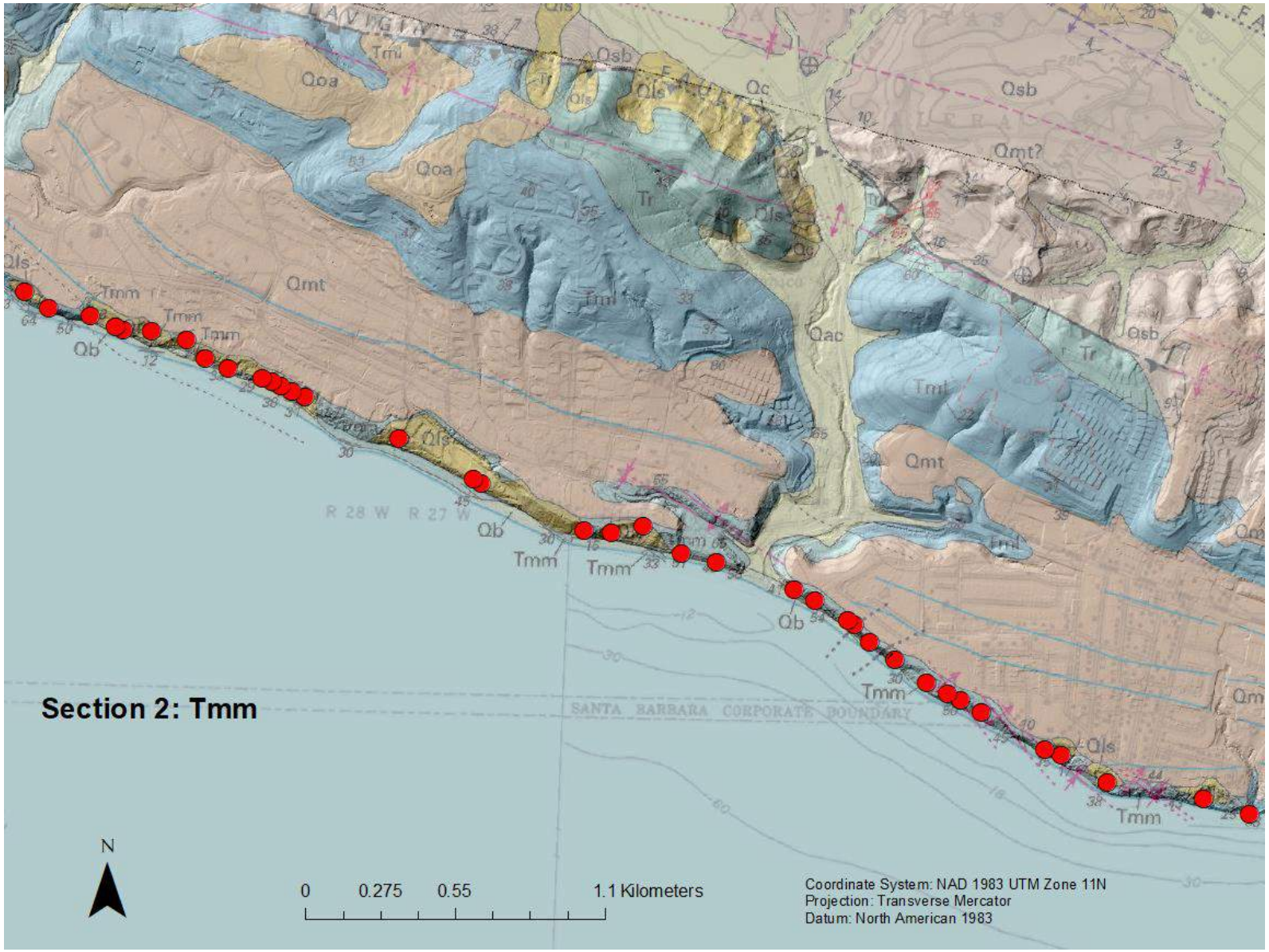
Section 2: Tmm
Qoa
Tml
Qsb
Qls
Qc
Qmt?
Qmt
Tr
Qac
Tmm
Qb
SANTA BARBARA CORPORATE BOUNDARY
R 28 W
R 27 W
N
0
0.275
0.55
1.1 Kilometers
Coordinate System: NAD 1983 UTM Zone 11N
Projection: Transverse Mercator
Datum: North American 1983

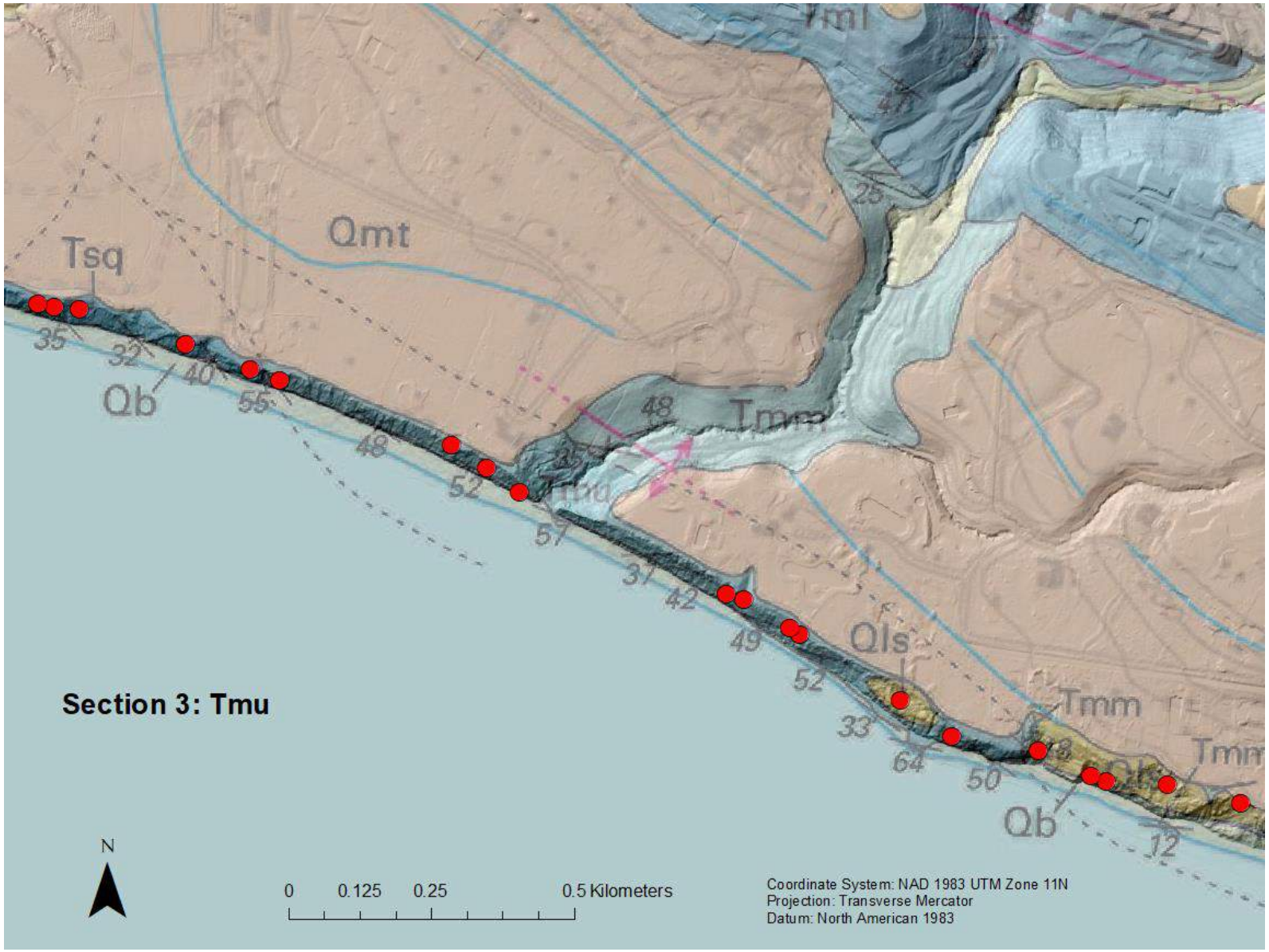
Tsq
Qmt
Qb
Tmm
Qls
Tmm
Qb
Tmm
35
32
40
55
48
52
57
37
42
49
52
33
64
50
12
Section 3: Tmu
N
0
0.125
0.25
0.5 Kilometers
Coordinate System: NAD 1983 UTM Zone 11N
Projection: Transverse Mercator
Datum: North American 1983

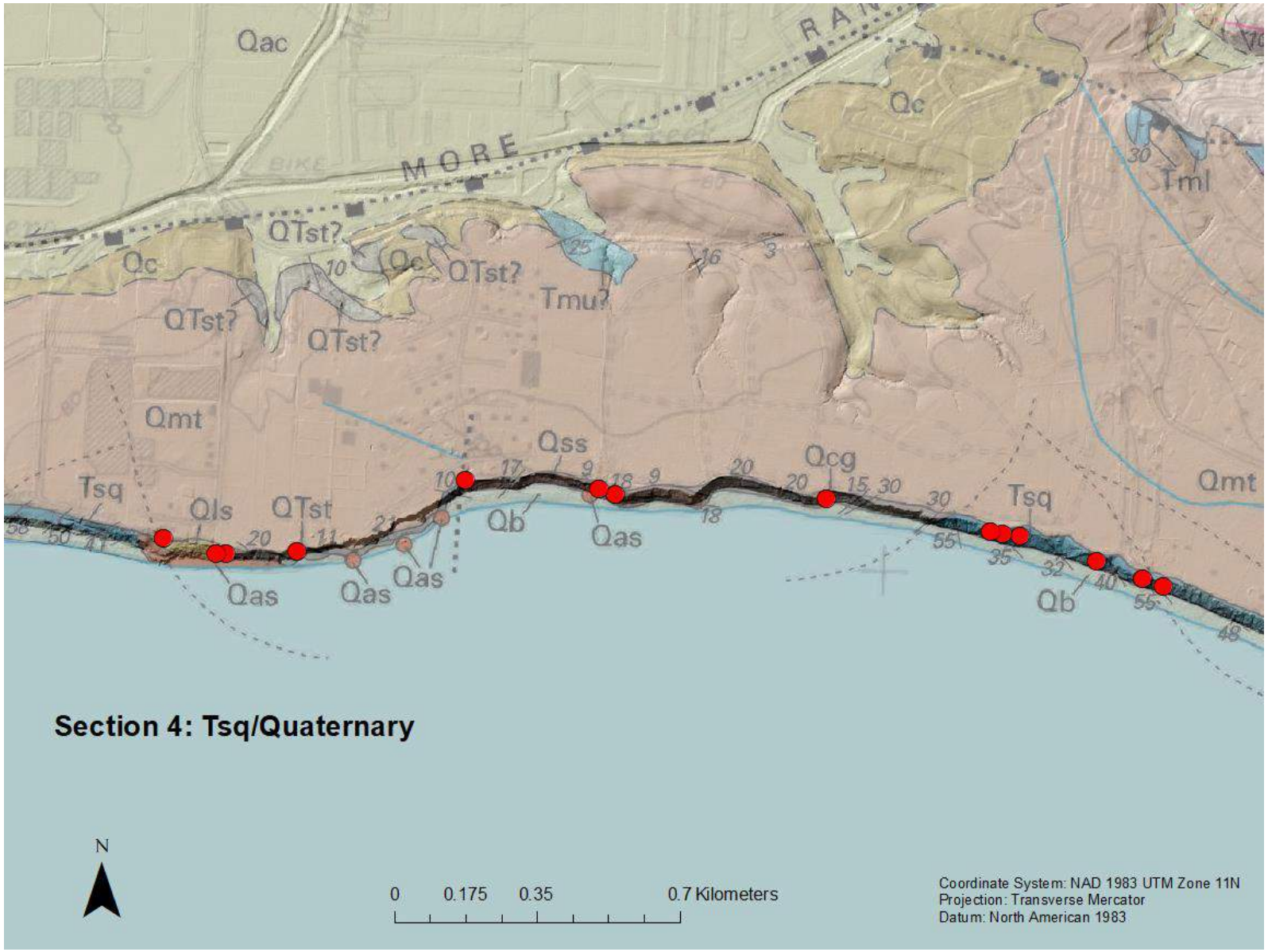
Qac
MORE
Qc
Tml
QTst?
Qc
QTst?
Tmu?
QTst?
QTst?
Qmt
Qss
Qcg
Tsq
Qls
QTst
Qb
Qas
Qas
Qas
Qas
Tsq
Qmt
Qb
Section 4: Tsq/Quaternary
N
0
0.175
0.35
0.7 Kilometers
Coordinate System: NAD 1983 UTM Zone 11N
Projection: Transverse Mercator
Datum: North American 1983

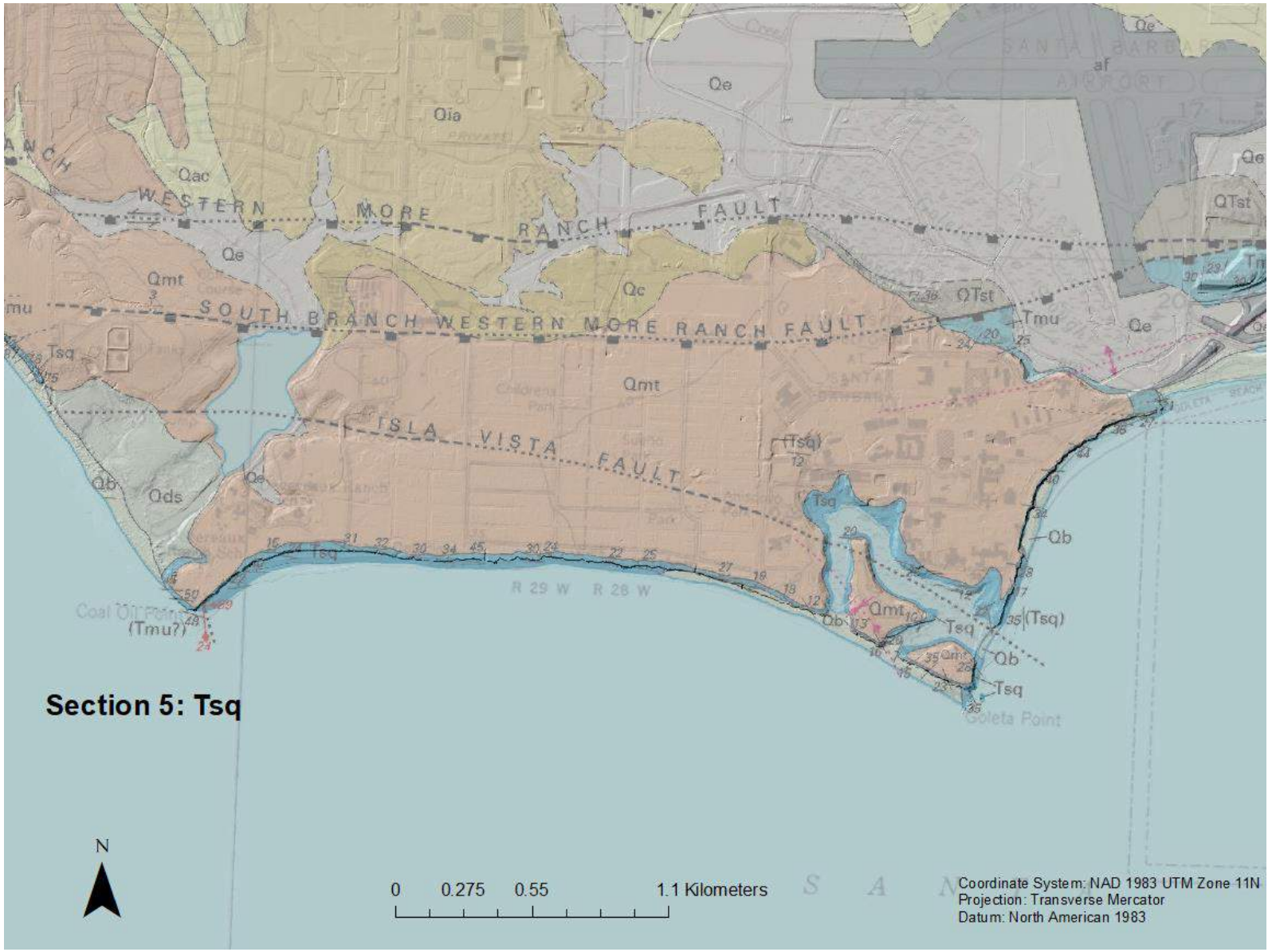
Qe
Qia
Qac
WESTERN MORE RANCH FAULT
Qe
Qmt
Qc
SOUTH BRANCH WESTERN MORE RANCH FAULT
Tsq
Qmt
ISLA VISTA FAULT
(Tsq)
Qb
Qds
Qe
Tsq
Qb
(Tmu?)
R 29 W
R 28 W
Qmt
Tsq
(Tsq)
Qb
Tsq
Qe
af
QTst
Tmu
Qe
Qe
Qb
Section 5: Tsq
N
0
0.275
0.55
1.1 Kilometers
Coordinate System: NAD 1983 UTM Zone 11N
Projection: Transverse Mercator
Datum: North American 1983